*Andean Geology 50 (3): 346-371. September, 2023*
doi: 10.5027/andgeoV50n3-3653

***Andean Geology***
*www.andeangeology.cl*

# Review of bomb and ash flows: Genesis and case studies of a subset of block and ash flow deposits

**Guillermo E. Alvarado[1], *Theofilos Toulkeridis[2], Yasuo Miyabuchi[3], Wendy Pérez[4]**

[1] *Geociencias, Instituto Costarricense de Electricidad, Apdo. 10032-1000, San José, Costa Rica.*
*galvaradoinduni15@gmail.com*
[2] *Universidad de las Fuerzas Armadas ESPE, P.O.BOX 171-5-231B, Sangolquí, Ecuador.*
*ttoulkeridis@espe.edu.ec*
[3] *Center for Water Cycle, Marine Environment and Disaster Management Kumamoto University, Kurokami 2-39-1, Chuo-ku, Kumamoto 860-8555, Japan.*
*miyabuchi@gmail.com*
[4] *Erwatec Ingenieurgesellschaft mbH, Edisonstrasse 62, 24145 Kiel, Germany.*
*wenppf@yahoo.com*

* *Corresponding author: ttoulkeridis@espe.edu.ec*

**ABSTRACT.** Pyroclastic density currents with an abundance of cauliflower-shaped bombs are an uncommon type of deposit, called bomb and ash flow (BoAF) deposits in several papers. Although they are similar to block and ash flow (BAF) deposits (*e.g.*, rich in juvenile blocks and breadcrusted bombs), they are often related to eruptions of mafic to intermediate magmas. In the current study, we analyze and compare historical and prehistorical BoAF-generating eruptions at Asama and Aso (Japan), Mayon (Philippines), Mt. Spurr (United States), Fuego (Guatemala), Arenal (Costa Rica), Cotopaxi and Tungurahua (Ecuador), and Láscar and Tilocálar volcanoes (Chile). Our review indicates that BoAFs show a substantial contribution of juvenile rounded material but with different rheologies and fragmentation mechanisms. This juvenile material is typically basaltic or andesitic, as it is more susceptible to form volcanic bombs with scoriaceous cauliflower textures. Thus, BoAFs could be a subset of the BAF deposits. The study and recognition of this type of deposit in volcanic sequences could be misinterpreted as a ballistic bomb deposit or even a hot bomb-rich lahar deposit, therefore, its appropriate interpretation is fundamental for volcanic hazard assessment.

*Keywords: Basic to intermediate PDCs, Cauliflower and breadcrust bombs, Lava pools, Strombolian, Active volcanoes, Volcanic hazards.*

**RESUMEN. Revisión de flujos de bombas y cenizas: Génesis y estudios de casos de un subconjunto de flujos de bloques y cenizas.** Las corrientes de densidad piroclástica con abundancia de bombas en forma de coliflor son un tipo de depósito poco común, denominado depósitos de flujos de bombas y cenizas (BoAF) en varios artículos. Aunque son similares a los depósitos de flujo de bloques y cenizas (BAF) (*e.g.*, rica en bloques juveniles y bombas con corteza de pan), a menudo se generan durante erupciones de magma máfico a intermedio. En el estudio actual analizamos y comparamos casos históricos y prehistóricos en Asama y Aso (Japón), Mayon (Filipinas), Mt. Spurr (Estados Unidos), Fuego (Guatemala), Arenal (Costa Rica), Cotopaxi y Tungurahua (Ecuador), y los volcanes Láscar y Tilocálar (Chile). BoAFs son el miembro final de procesos donde hay un aporte sustancial de material juvenil redondeado, pero con diferentes estados reológicos y mecanismos de fragmentación e, incluso, geoquímica y petrográficamente, pues los basaltos y las andesitas son más susceptibles de formar depósitos ricos en bombas escoriáceas con texturas en coliflor. Por lo tanto, el depósito BoAF podría ser un subconjunto del depósito BAF. El estudio y reconocimiento de este tipo de depósito en secuencias volcánicas podría ser mal interpretado como un depósito de bombas balísticas o incluso un depósito de lahar caliente rico en bombas, por lo que su adecuada interpretación es fundamental en la evaluación de peligros volcánicos.

*Palabras clave: PDC básicos a intermedios, Bombas coliflor y corteza de pan, Piscinas de lava, Estromboliano, Volcanes activos, Peligros volcánicos.*

## 1. Introduction

Pyroclastic density current (PDC) deposits are commonly described in two major types: a) ignimbrites or pumice flows, and b) block-and-ash flows (BAFs) (*e.g.*, Branney and Kokelaar, 2002; Burgisser and Bergantz, 2002; Sulpizio *et al*., 2014). More recently, the ignimbrites that originated from the collapse of single point-source eruption columns, usually smaller than 1 km$^3$, are named "Vulcanian ignimbrites" and "Plinian ignimbrites" depending on the style of the eruption they are associated with, whereas the larger ones are named "caldera-forming ignimbrites" (Giordano and Cas, 2021). The vulcanian ignimbrites differ in the percentage of larger clast components (bombs *versus* juvenile blocks) from small-volume PDCs (<1 km$^3$; Wright *et al*., 1980) such as dilute PDCs (phreatomagmatic base surges and lateral blast) or BAFs (Brown and Andrews, 2015; Giordano and Cas, 2021). However, small-volume PDCs do not include several other deposits characterized by a high vesicularity coarse grain fraction (*i.e.*, scoriaceous bombs, cauliflower bombs, spatter bombs, and coarse lapilli), which are also comparatively richer in non-juvenile blocks than BAFs. These are the so called "scoria-and-ash flows" (Wright *et al*., 1980; Gourgaud *et al*. 2000; Bernard *et al*., 2014; Andronico *et al*., 2018), spatter-rich pyroclastic flows (Mellors and Sparks, 1991), bomb-and-ash flows (BoAF), bomb-rich pyroclastic flows, or PDC deposit of cauliflower bombs (Gardeweg *et al*., 1998; Alvarado and Soto 2002; Miyabuchi *et al*., 2006; Benage *et al*., 2014).

The traditional (and most cited) BAFs are generated either by the gravitational collapse of unstable portions of lava domes, or by the explosive decompression, and disruption of pressurized interiors of andesitic to rhyodacitic lava domes (Fink and Griffiths, 1998; Lube *et al*., 2007; Felix and Thomas, 2004; Dufek *et al*., 2015; Brown and Andrews, 2015) or lava front collapse (Cas and Wright, 1987). The BAF deposits consist predominantly of dense, non- to poorly vesicular juvenile clasts derived mainly from the fragmentation of a lava dome. The juvenile clast may be prismatically jointed blocks, which indicate hot emplacement or breadcrusted juvenile blocks (Brown and Andrews, 2015).

On the other hand, BoAFs have a ubiquitous abundance of bulbous cauliflower bombs (Alvarado and Soto, 2002), also called slightly flattened globular-shaped clasts (Yasui and Koyaguchi, 2004), or "pancakes". The latter is an informal term for large volcanic bombs characteristically flat and disk-shaped (length and width are about five times the thickness) with a bread-crusted texture (Douillet *et al*., 2013), or even for rounded black scoria blocks (Andrade *et al*., 2005). At first glance, there is a superficial and textural difference between both deposits (Fig. 1), in which the PDC deposit rich in juvenile blocks is the end member of a typical BAF deposit. Instead, the bomb-rich PDC, on the other hand, suggest that it could be the end member of more unusual BoAF deposits, topic that will be discussed in this work.

Despite their frequent occurrence and observations during recent eruptions at Arenal (Alvarado and Soto, 2002), Tungurahua (Douillet *et al*., 2013; Hall *et al*., 2013; Romero *et al*., 2017), and Fuego (Escobar, 2013) volcanoes, and their existence in prehistoric deposits, most of the BoAF deposits are described simply as BAFs (Moore and Melson, 1969), or have been even misinterpreted as bomb fall deposits (Ureta *et al*., 2021). Therefore, these bomb-rich deposits in old volcanic sequences are underrepresented in the literature and their interpretation is still problematic. We have documented examples of BoAF deposits in ten volcanoes in seven countries (including seven well-documented historical cases) to understand and highlight their genetic processes and to recognize their contrasts with well-known BAFs and scoria-and-ash flow deposits. The primary intent of this paper is thus to stimulate discussion around this topic and to prompt a reappraisal of studies of small-volume, coarse PDCs, providing a better understanding of their eruption dynamics and genesis.

## 2. Methodology and terminology

We reviewed the literature on BAFs, and possible deposits associated with BoAFs elsewhere (Alvarado and Soto, 2002; Murcia *et al*., 2013). In addition, field visits were carried out to several volcanoes with extensive studies on both types of deposits (*e.g.*, Japan, Ecuador, Chile, and Costa Rica). In addition, we contacted several authors who studied similar deposits in other countries like Indonesia and Guatemala.

The *juvenile blocks* (>6.4 cm in diameter) are those poorly or non-vesicular or microvesicular magmatic fragments (also known as cognate lithics), usually dense, angular to subangular,

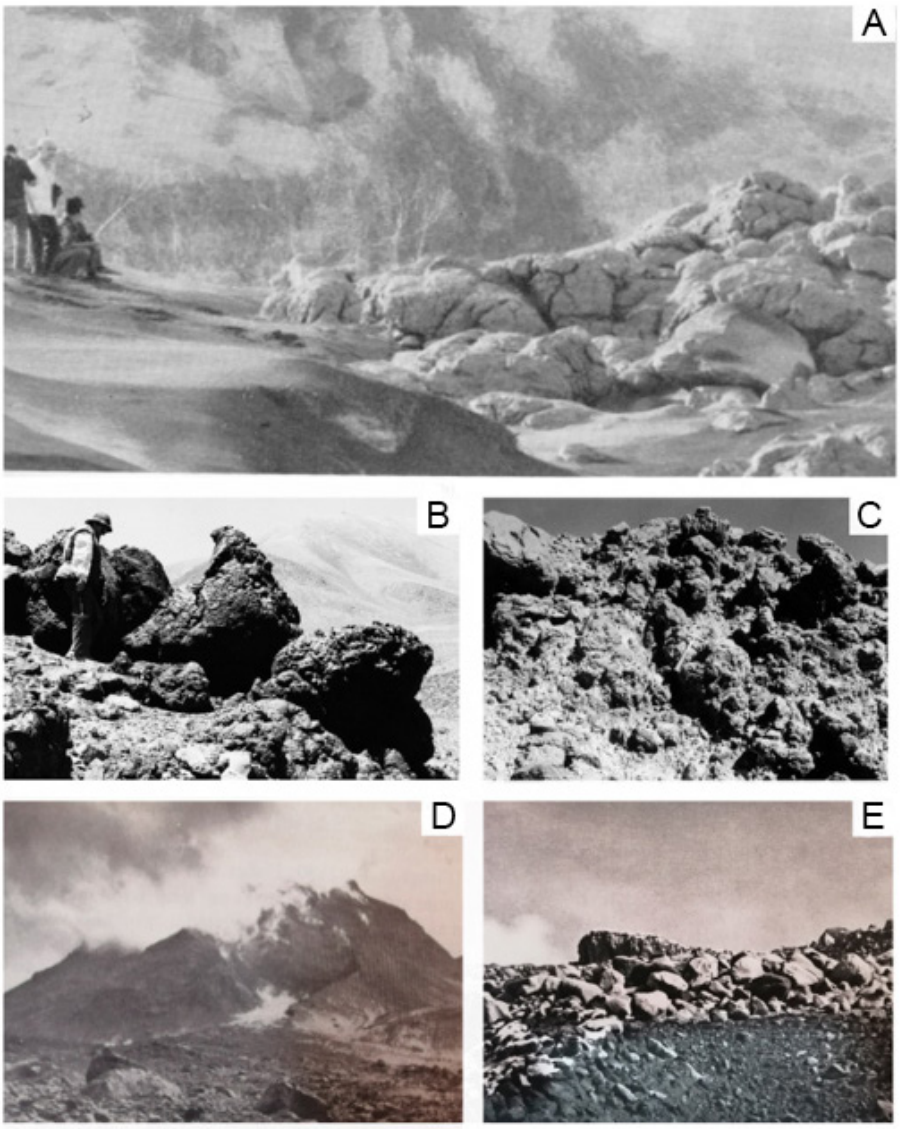


FIG. 1. Historical examples from the literature in which, from a first glance, is possible to dilucidate the difference between a PDC deposit rich in bombs as bomb and ash flow deposits (BoAF), examples A, B and C, and PDC mainly composed by juvenile angular clast, typical of block and ash flow (BAF) deposits as D and E examples. **A.** 1968 PDC, Mayon volcano, Moore and Melson (1969). **B.** Lower Chaile PDC, Lascar volcano, Gardeweg *et al.* (1998). **C.** Saltar PDC, Lascar volcano, Gardeweg *et al.* (1998). **D.** 1976 eruption of Augustine volcano, Alaska, Fisher and Schmincke (1984). **E.** Sheveluch volcano in Kurile Islands, Russia, Green and Short (1971).

sometimes exhibiting distinctive prismatic jointing, and breadcrust structures or expansion cracks, which are indicative of hot emplacement. The *non-juvenile* components are fresh or hydrothermally altered block-size accessory lithics, sometimes with oxidized rims, but lithologically distinct from the juvenile material, representing rock fragments which were incorporated into the flows. The term "bomb" is based on granulometric classification of juvenile vesiculated ejecta (>6.4 cm in diameter), irrespective of their primary origin, and not only related to a ballistic fragment (Cas and Wright,

1987; Murcia *et al*., 2013). In our case study, they vary from scoriaceous cauliflower to breadcrust bombs, of which some appear flattened or in a disk-shaped form, rich in vesicles and with evidence of molten or plastic behaviors. Since there is still an entrapment in the volcanological community of using the term "bomb" to describe ballistics, many bombs in PDC deposits were described as scorias, scoriacerous blocks, rounded black scoria blocks, cauliflower crust blocks, cauliflower-like blocks, molten clots, or even breadcrust blocks or blocks alone. This situation of referring to the bombs (*i.e.*, large vesiculated juvenile clasts) as blocks, and in several cases not including photographs or componentry (juvenile and non-juvenile blocks, bombs, matrix, etc.) has hindered the distinction between BoAF and BAF deposits.

We used the term lava pool as the transient or temporary lava that fills the open crater vent at the summit of a stratovolcano (*sensu* Tazieff, 1994), which overflows more or less continuously but never lasts longer than the eruptive episode, usually with a thicker and more rigid crust. Consequently, lava pools should not be equivalent to the permanent lava lakes defined as >100 $m^2$ of molten lava at the vent for a long-time interval (Lev *et al*., 2019), usually extending beyond a single eruptive cycle. Lava pools (*sensu* Tazieff, 1994) are also different to lava ponds (or passive lava lakes), where lava flowed away from the active vent and filled a topographic depression before quenching (Tazieff, 1994; Lev *et al*., 2019). The term lava pool, although not very frequently used in the volcanological literature, could be useful to explain several processes observed in open conduit eruptions that will be explained in the following text.

## 2.1. Review of eruptions producing small volume PDCs rich in bombs

We examined seven contemporaneous and five prehistorical cases of small-volume bomb-rich PDC deposits in order to understand their origin and emplacement mechanisms. These historical cases are the key to the interpretation of analogous ancient deposits as described later (Figs. 2, 3 and 4).

### *2.1.1. Cotopaxi volcano, Ecuador*

The PDC deposits are present in narrow valleys and form small fans at the foot of the edifice. Morphologically, they show finger-shaped flows with lateral bomb-rich *levées* (0.5-1.5 m-high), and a 2 m-high flow front. The deposit is massive, poorly sorted, with black to dark gray cauliflower and breadcrust bombs and angular blocks up to 7 m in diameter set in a fine non-cohesive matrix with reverse grading (Figs. 3C, D; 4C; 5B). At least 75 vol.% of the clasts in the deposit correspond to decimeter- to meter-sized juvenile blocks, and also large spherical- to elongated-shaped bombs, with cauliflower surfaces. The juvenile material is andesitic (Andrade *et al*., 2005). Bombs were deformed or wrapped up plastically around blocks. The juvenile blocks are poorly vesiculated, but in many cases, some juvenile fragments have a dual textural character with a cauliflower to breadcrusted surface They have a transitional contact between the two, while often exhibiting cracked open joints with variable percentages of vesicles, some being "spongy" or vesicular. On the other hand, the light-gray non-juvenile andesitic blocks are poorly vesicular, with subangular to subrounded shape, frequently displaying a rusty surface These lithic fragments comprise an estimated modal abundance of >30% in the matrix.

Locally overlying the 1877 BoAF deposits, there is a reddish block-rich debris flow deposit, rich in reworked bombs and with degassing pipes. Pistolesi *et al*. (2011, 2013) interpreted the frequent occurrence of chilled margins around bombs as interaction of the juvenile hot material with ice and water.

Pistolesi *et al*. (2011, 2013) also described PDC deposits associated with the 1766-1768 and 1853 events, which are preserved on the northern and southern flanks of the volcano. These deposits partially fill the narrow gullies of the cone and spread over the flanks forming tongue-like deposits with low *levées* (Fig. 3D). The maximum runout distance varies from 6 to 12 km and covers an area of ~$8\times10^5$ $m^2$, with an average thickness of ~2 m (total volume ~$1.6\times10^6$ $m^3$). These PDC deposits are matrix-supported scoria bomb- and block-bearing, with dark (black to greenish in color) cauliflower scoria bombs and blocks up to 1 m in diameter, which are concentrated around a central, matrix-rich body containing green pumice fragments embodied in fine to coarse ash, comparable to those of 1877.

### *2.1.2. Asama volcano, Japan*

Asama (2,568 m a.s.l.) is the most active volcano of Honshu Island, Japan, and one of the best documented

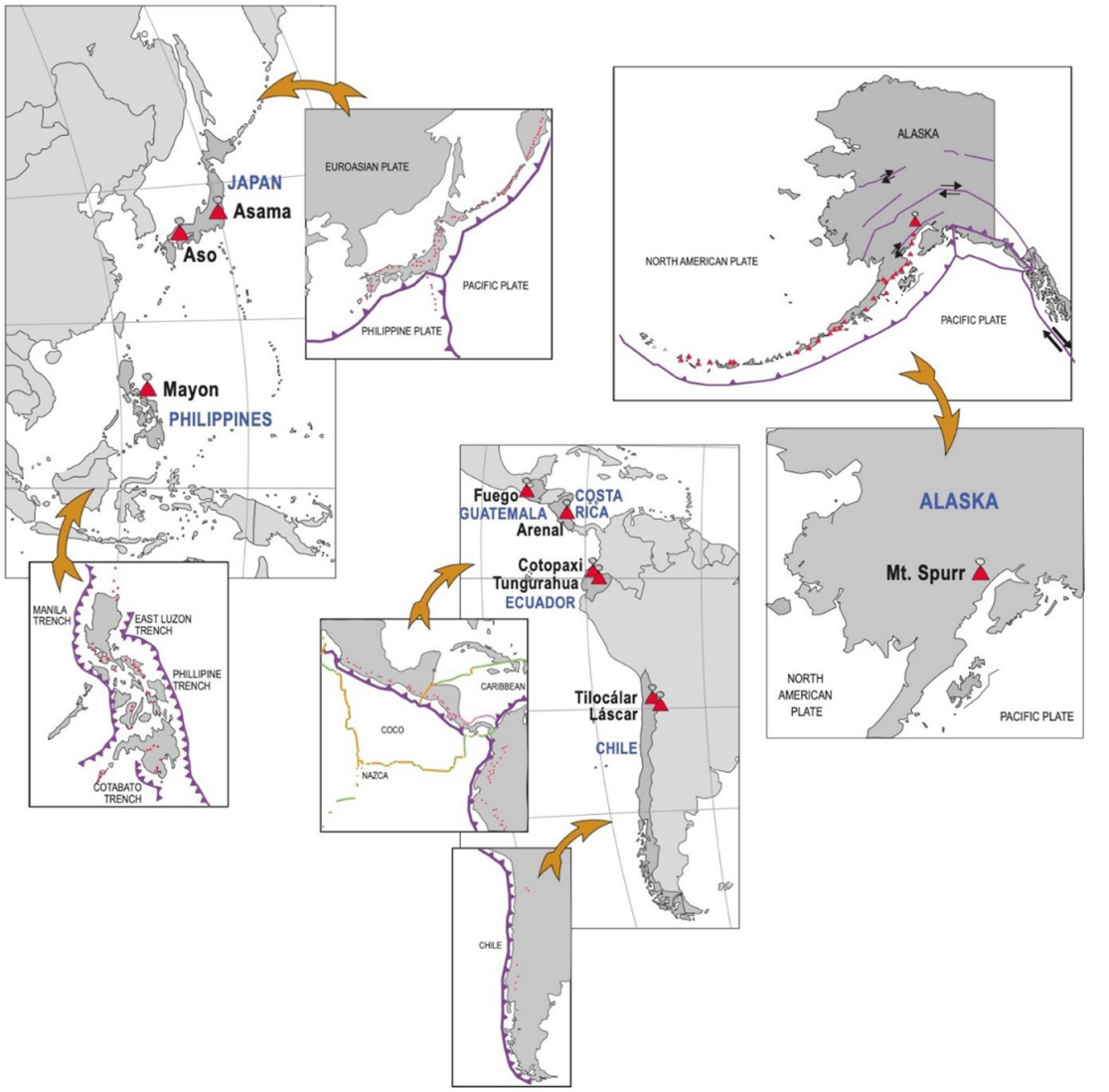


FIG. 2. Map with the location of the volcanoes described in the text: Asama, Aso, Mayon, Mt. Spurr, Fuego, Arenal, Cotopaxi, Tungurahua, Láscar and Tilocálar.

with the longest recorded eruption history (Fig. 2). The largest and most destructive eruption in the past 1,000 years in Japan occurred at Asama in 1783, when it erupted for three months producing pumice fallout of andesitic composition, PDCs (including the Agatsuma PDC), and lava flows. The eruption built a cone. The Agatsuma PDC deposits are widely distributed toward the northeast up to 8 km from the vent, having a complex stratigraphy with a strong facies variation (Aramaki, 1956, 1957; Yasui and Koyaguchi, 2004). Within the vertical section, the middle and upper units of the PDC sequence are characterized by blocks and bombs, particularly the upper unit that developed notable reverse grading, with a bomb-rich zone that is clast-supported to the top. These units contain dark brown ash and small amounts of oxidized interstitial ash, and are matrix supported at the base, almost depleted in large bombs. The deposit contains cauliflower to breadcrust bombs (Fig. 4E, F). These are slightly

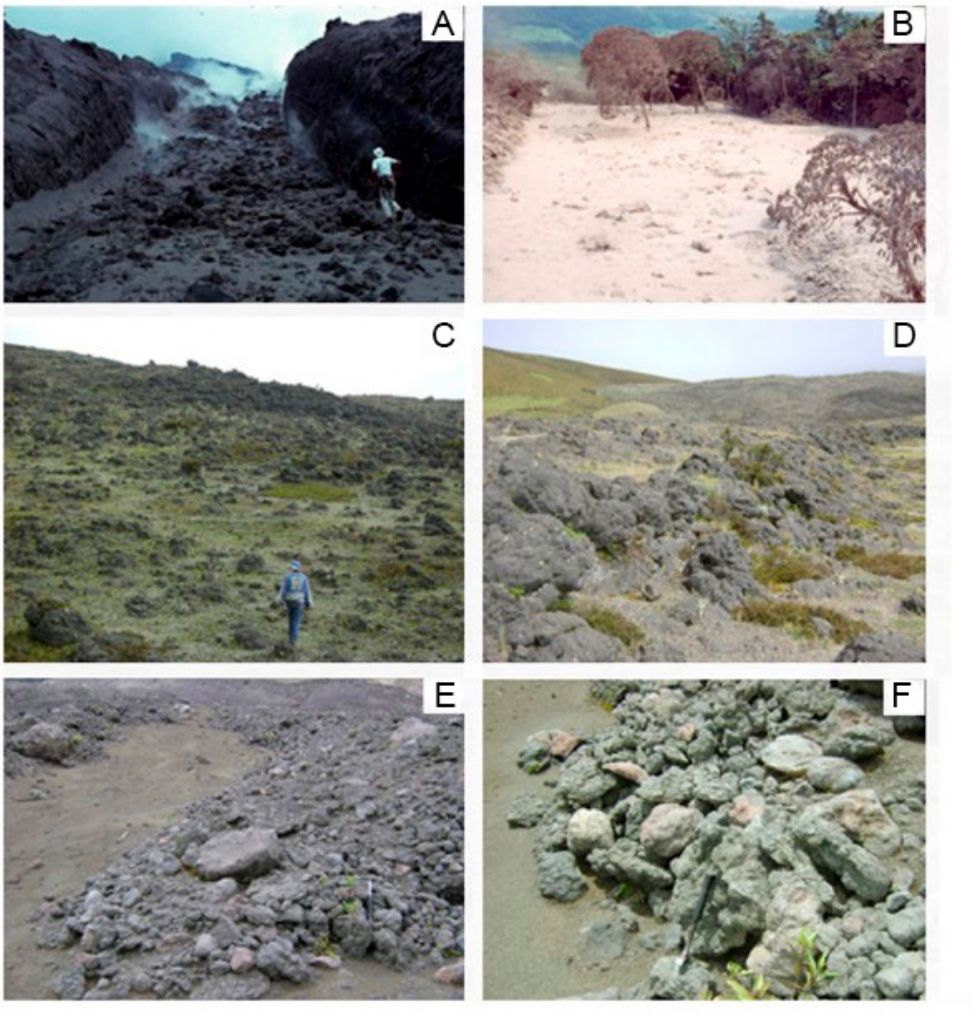


FIG. 3. Different views of the BoAF deposits and their morphologies. **A**. Polished and striated lava flow channel resulting from a channelized PDC at the middle part of the volcano (Arenal, 1975). **B**. A few hours after the PDC, the surface was very hot and rich in fine ash (fall and dilute PDC) deposits, which was washed away during the first heavy rains (Arenal, 1998). **C**. Bomb field more than one century later (Cotopaxi, 1877). **D**. Levee composed of bombs (Cotopaxi, 1877). **E**. PDC front and tongue (Tungurahua, 2006). **F**. Lateral levee rich in clast-supported bombs (some flattened in shape) and blocks with imbricate structure. (**E**-**F**), which look like a rubbly lava flow, correspond to "pancakes" bombs in a PDC deposit, an informal term (*sensu* Douillet *et al*., 2013) for large clasts characteristically flat and disk-shaped with a bread-crusted texture.

flattened, globular-shaped with rather smooth and reddish-brown surfaces, which are typically less than 1 m in diameter and display radial cooling joints. The deposit is composed of irregular bombs and the ash matrix has different degrees of welding. Other features are tree casts left by burned trees surrounded by deformed pyroclastic material also known as secondary charring. Some of the bombs (up to 9 m in the long axis), are plastically deformed with reddish brown interstitial ash. Some flow units preserve a remarkable lobe-like topography (ridges) and *levées* (Aramaki 1956, 1957; Yasui and Koyaguchi, 2004).

### *2.1.3. Mayon volcano, Philippines*

Mayon volcano (2,462 m a.s.l.; Fig. 2) and its well-known eruption in 1968 was described in detail by Moore and Melson (1969). The resulting pyroclastic deposits were classified as BAFs, whereas Wright *et al*. (1980) classified it as a scoria and ash flow deposits. On April 21, and by May 15, 1968, more

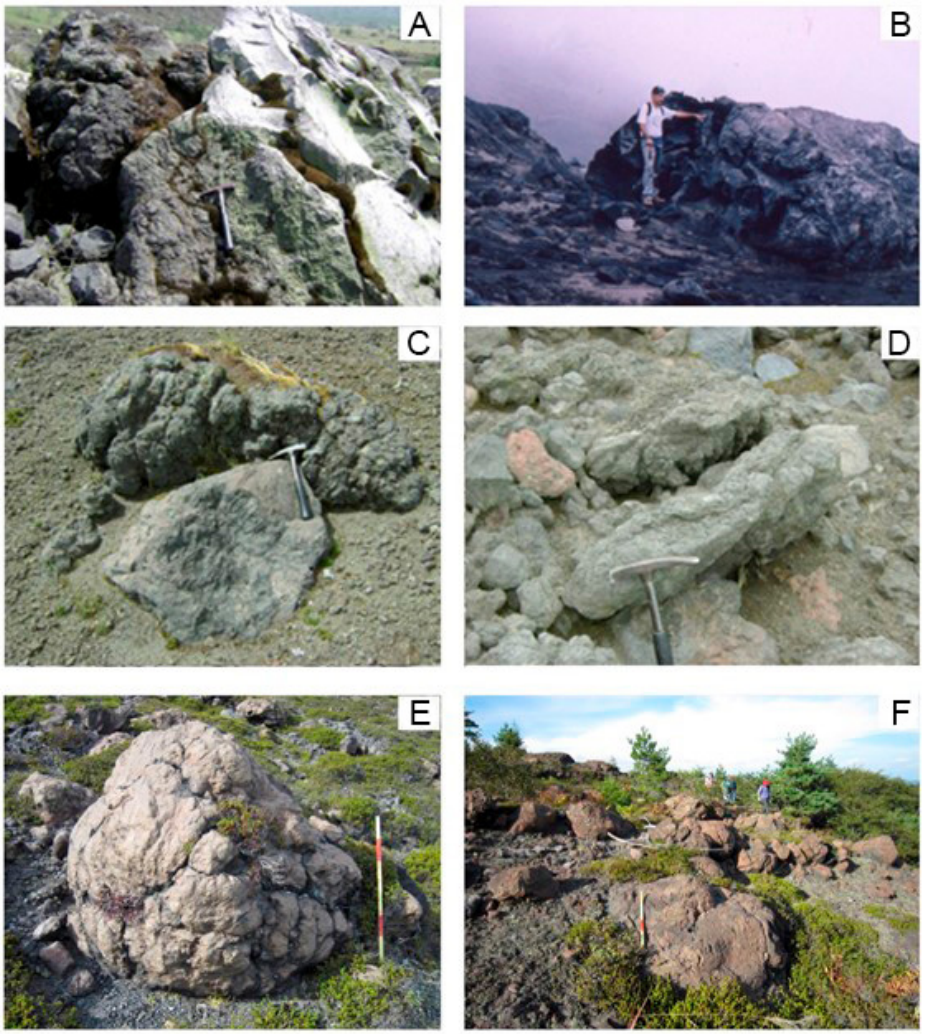


FIG. 4. Examples of cauliflower bread-crusted bombs in historical BoAF deposits. **A**. Cauliflower bomb (left) with juvenile block (right), and in the foreground, a bokken bomb (Arenal, 1993). **B**. Large bombs with cauliflower texture (Arenal, 2000). **C**. Bomb with a slightly plastic deformation attached to a non-juvenile block (Cotopaxi, 1877). **D**. Flattened bombs with imbricate structures (Tungurahua, 2006). **E-F**. Cauliflower bomb and bomb deposits (Asama, 1783 Agatsuma PDC). The hammer is 28 cm long.

than a hundred explosions produced PDCs and lava flows, accompanied by 3- to 10-km vertical ash clouds. The resulting PDC deposits were unconsolidated, poorly sorted and unlayered, containing crystal-rich ash, scoriaceous and poorly vesiculated lapilli, as well as blocks (mainly juvenile) and bombs. The juvenile clasts are angular, but many of them exhibit a characteristic rounded or lobated cauliflower textured surface concentrated to the top (Fig. 1A); they are ~3.5 times more abundant than the angular blocks and averaging about 30 cm in diameter. On their outer surfaces, the cauliflower bombs are scoriaceous, rarely pumiceous, and the vesicles show a uniform increase in vesicularity from the center to the margin, although other juvenile clasts have a denser margin with an irregular scoriaceous core. The deposit made of several flow units has a thickness between 4 and 7 m and an estimated volume of $15\times10^6$ $m^3$. The velocity of the flows ranged from 9 to 63 $ms^{-1}$. The largest PDC descended to the southwest flank and reached 4-5 km from the summit, although the seared zone was at 7 km (Moore and Melson, 1969). The

photographs and description by Moore and Melson (1969) demonstrated that the most abundant clasts were cauliflower bombs.

### *2.1.4. Mount Spurr volcano, United States*

Crater Peak is a 2,309 m a.s.l. satellite cone on the south flank of the Mount Spurr volcano, ~125 km west of Anchorage. The August 18, and September 16-17, 1992, eruptions generated very coarse, fine-depleted, poorly sorted, and clast supported PDC deposits. Most clasts (60-80 vol.%) consist of dense to slightly, some highly vesiculated (15-20% vesicles) bombs, dark gray to brownish black compositionally homogeneous, porphyritic juvenile andesite (56-57% $SiO_2$). The bombs have a characteristic orbicular shape with irregular cauliflower-like exteriors and slightly breadcrusted surfaces, as they fractured developing polygonal joints. Accessory and accidental clasts correspond to fragments of lava but include some vesiculated metasedimentary rocks. Well-developed *levées* and surface ridges are present along the margins of the deposit, and at topographic depressions it attained a maximum thickness of 1-3 m. At depositional areas, the deposits form steep lobate flow fronts with heights from 1 to 1.5 m. The current traveled a maximum distance of about 3.2 km and has a combined bulk volume of about $4\times10^5$ $m^3$ (Miller *et al*., 1995).

Field characteristics indicate that the August 18 PDC (and probably those of September 16-17) began as slow-moving hot avalanches. The distribution of the small-volume PDC deposits indicates that they did not result from boiling-over through low points on the crater rim or through column collapse because apparently no PDC traveled through the lowest point of the Crater Peak rim. Thus, they may have been generated, at least in part, by directed ballistic ejection and the collapse of an inclined column (Miller *et al*., 1995).

### *2.1.5. Arenal volcano, Costa Rica*

Arenal is a small (1,657 m a.s.l., Fig. 2) Holocene basaltic andesite stratovolcano that was continuously active from 1968 to 2010. A new cone was formed on crater 'C', which was the highest crater of the three new explosive craters opened in 1968. Crater 'C' widened from a 60-m-diameter circular shape in early 1980 to a slightly elongated shape of some 150-200 m in diameter in 1993, which contained a small lava pool. The pool's crust was frequently fragmented by sudden Strombolian and Vulcanian explosions. Periodically, small and ephemeral spatter cones were formed at the crater rim.

During the eruptions on 17 and 21 June 1975, PDCs descended the northwest flank of Arenal along the northern valley, reaching a length of ~3.6 km. The deposits on the lower and middle section were between 8 to 10 m thick and consisted of ~20-30% large angular blocks of up to 8 m in size in a matrix (~30-50%) of a heterogeneous poorly sorted mixture of very coarse- to fine-grained angular lapilli and ash. There were also cauliflower bombs (25-50%), of which many of them showed surface joints with scoriaceous rims. Plastic deformation and fragmentation by impact observed in the deposit, as well as flattening after the deposition, suggest a high temperature emplacement; however, the temperature of the ash-cloud associated with the PDCs was relatively low (about 200 °C), as most of the vegetation was not charred. The PDCs were highly erosive in the upper valley, particularly on steep higher flanks, as indicated by the presence of grooves and striations (Fig. 3A). The estimated volume of the 1975 PDC deposit was ~$1\text{-}2\times10^6$ $m^3$ (Alvarado and Soto, 2002). A new significant PDC occurred in 1993. Eyewitnesses reported repeated rockfalls restricted to the upper flanks of the volcano prior to the main event.

Another PDC on August 28, 1993 moved down the slope from crater 'C' and was channeled between the *levées* of old lavas. The deposit formed a fan-shaped, trilobate apron about 500 m wide, extending up to 3 km from the vent. Each lobe was between 50 to 100 m in width, with a thickness of 1 to about 10 m, consisting of blocks and bombs with a surrounding zone of directed dilute PDC deposits. There was a definite small (<1.5 m high) flow front and bomb-rich *levées* (0.5-1.5 m high) with scarce fine material. The intra-*levée* channels contained fine ash mixed with large dense blocks and bombs. The deposit was massive, poorly sorted, with black to dark gray bombs and angular blocks of up to 7 m in diameter, set in a fine non-cohesive matrix. Between 75 and 90 vol.% of the clasts in the deposit were large (decimeters to meters in diameter) juvenile blocks, and large spherical- to elongated-shaped bombs, with cauliflower and breadcrust surfaces (Fig. 4A). Due to the relative fluidity of the bombs, their shapes were modified during transport and emplacement within the flow. As an example, figure 4B demonstrates flattening after

the deposition. The molten behavior of the bombs is also demonstrated by deformation of the blocks around other blocks or large trees, which some of the latter were partially carbonized. The bombs also often had cracked open joints (*i.e.*, post depositional open fractures) with a variable percentage of vesicles (20-35% and more), of which some were "spongy" or filamentous scoria (density 1.2-1.6 g $cm^{-3}$). Some bombs even collapsed and flowed for one meter. The outer parts of the bombs were slightly more vesicular (1.65 g $cm^{-3}$) than their interiors, with a mean density of 1.5-1.9 g $cm^{-3}$. The poorly vesiculated juvenile blocks (density 2.5 g $cm^{-3}$) had an oblate form. In many cases, some juvenile fragments had a dual character, one face being non-vesiculated, blocky, and angular, and the other being cauliflower-like, with a transitional contact between the two. On the other hand, the light-gray non-juvenile blocks were poorly vesicular (density 2.3-2.8 g $cm^{-3}$), subangular to subrounded, some of them showing rusty surfaces and lacking evident cooling fractures (Alvarado and Soto, 2002; Cole *et al*., 2005). The 1993 particle-size distribution was strongly bimodal, with one mode in the range of decimeters to meters and the other in the ash, lapilli and small (<20 cm) bomb-block range (Fig. 5A). The deposits occurred in two main gradational facies (bottom-up) with a crude inverse grading. The massive, non-graded basal unit (between 25 and 100 cm in thickness) consisted of juvenile and non-juvenile blocks, some clast-supported small semi-spheric bombs with a poorly sorted matrix of pulverized scoria, fragmented dense rocks, ash, lapilli, bombs, blocks, and some organic matter, with no internal bedding. The upper part (up to 1.5 in thickness) was composed of cauliflower bombs and angular blocks set in a matrix (Alvarado and Soto, 2002).

Rockfalls were observed two days before the eruption when abnormal activity at Arenal during the night of 28 August 1993 was reported by many observers. A series of rockslides containing pieces of incandescent blocks developed slowly on the northwest and west flanks of the volcano after 19:50 local time from cone 'C', which lasted at least 50 minutes. At about 21:00, the walls collapsed (without an earthquake or accompanying explosion), with the outpouring of the lava pool transformed into an incandescent PDC. The duration of the PDC was of about only three minutes, according to the seismic record. An 80 m deep horseshoe-like opening was present in the crater wall immediately after the 1993 event, just in the area where intense fumarolic activity and repeated rockfalls had been observed two days before.

Later, on May 5, 1998, August 23, 2000, and March 24-26, 2001, between 23 and 27 PDCs (within each period) occurred at Arenal (Fig. 3B). Most of the coarse components of the deposits were made of faceted blocks, and between 5 and 50 wt% were cauliflower and breadcrusted bombs. Cole *et al.* (2005) pointed out that, generally, the maximum juvenile clast size decreased with distance from the source. In the proximal region, about 1.5 km from the crater, bombs 5-10 m across (some even 40 m across) were found (Fig. 4B). At the frontal lobes of the PDCs, bombs and blocks exceeding 1.5 m in size were rare (*e.g.*, August 2000, March 2001).

### *2.1.6. Tungurahua volcano, Ecuador*

Tungurahua is an andesitic stratovolcano (5,023 m a.s.l.) located ~140 km south of Ecuador's capital, Quito (Fig. 2). The eruptive chronology since the 13th Century accounts for at least seven PDC-forming cycles (including the most recent between 1999 and 2016). By July and August 2006 and May 2010, Tungurahua produced PDC forming eruptions, representing an increase in explosivity compared to the 1999 to 2006 Strombolian events, although one major eruption occurred in 2008. On 26 and 28 May 2010, another strong eruption sequence occurred, producing 1-3 km long PDCs on the north, northwest, west, and southwest flanks of Tungurahua (Le Pennec *et al.* 2008; Kelfoun *et al*., 2009; Hall *et al*., 2013, 2015; Romero *et al*., 2017). Without warning, Tungurahua generated PDCs on July 14th to 16th, 2006 accompanying VEI 2 Strombolian activity with occasional high energy bursts. The activity increased by August 16-17 2006. After midnight of August 16, an intense period was characterized by a powerful lava fountain up to 500-1,000 m above the crater, a >16-km-high eruption column (VEI 3), and the quasi-contemporaneous generation of the most voluminous PDC by column collapse recorded during this eruptive cycle, which descended into 17 different ravines and extended up to ~10 km from the crater towards the northwest, north, west and southwest. The death toll reached 6 people, while ash fall banned flights at various airports (Toulkeridis and Zach, 2017). The descent of the PDCs down the cone's steep upper flanks (~28°) favored air entrainment, increasing the fluidization of the

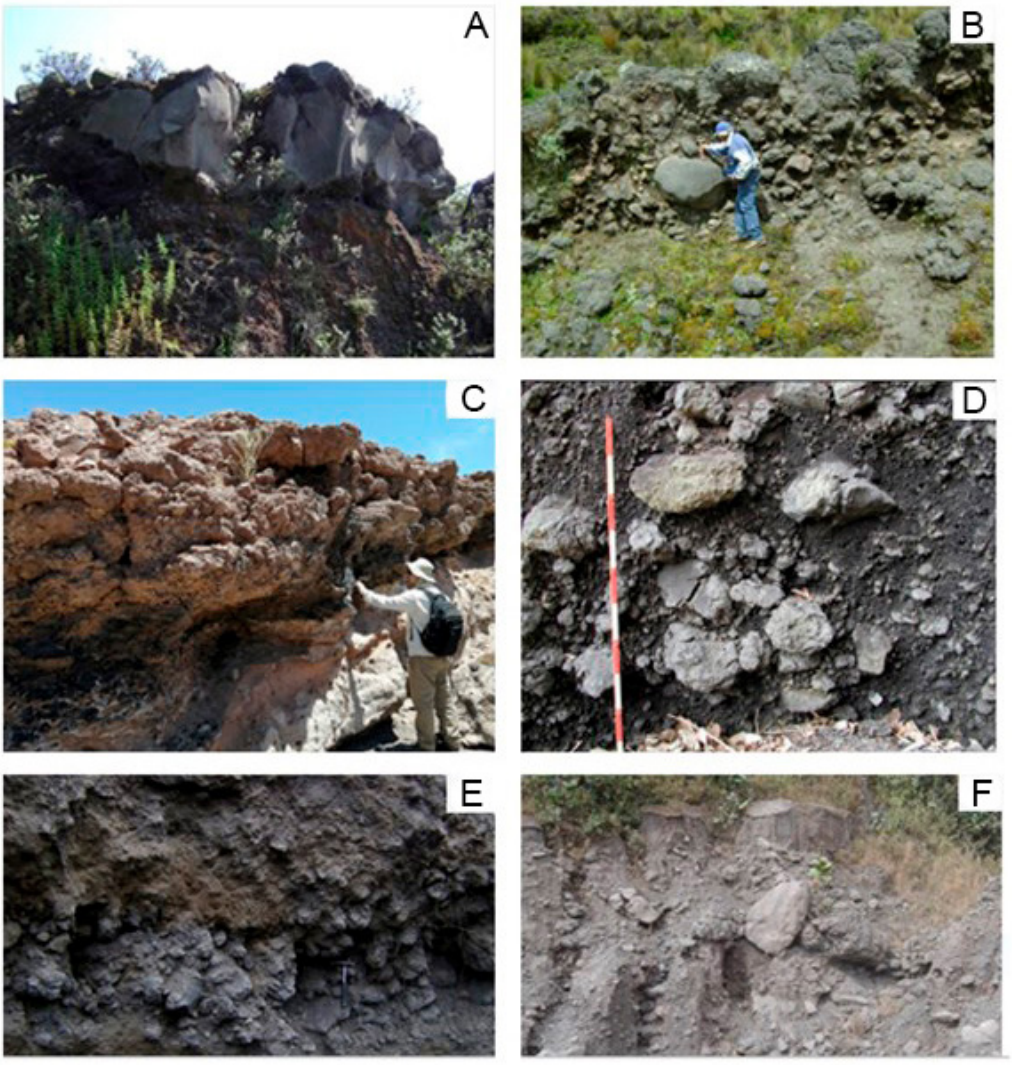


FIG. 5. Internal structure of the deposits. **A**. Large, flattened bomb at the top of the deposit (Arenal, 1993). **B**. Reverse grading in bombs but a large non-juvenile block at the base (Cotopaxi, 1877). **C**. Reverse grading BoAF deposit and in the lower part a spatter agglomerate layer (Tilocálar Sur volcano, 730 ka). **D**. Lower unit the Izumikawa PDC deposit (Aso, 19 ka). **E**. Internal crude layering (Tungurahua, prehistoric deposit). **F**. Cauliflower bombs and blocks (Fuego volcano, courtesy of R. Escobar).

current (Kelfoun *et al*., 2009; Hall *et al*., 2013). On January 30, 2014, a new eruptive phase begun with a climax on February 1st. The PDCs branched into at least nine ravines from the north, west and southwest flanks down to the base of the volcano (Romero *et al*., 2017).

In general, the PDC deposits described were composed of several facies associations depending on the topographic setting (Douillet *et al*., 2013; Romero *et al*., 2017), ranging from massive to cross-stratified, interpreted as PDCs that overbanked the gentle ridges of valleys of the upper part of the volcano deposits.

The total thickness varied from 3 to 5 m when these deposits filled topographic depressions. The surface of the massive deposits locally exhibited a fingered lobe-and-channel morphology. The lobes strictly followed topographic lows on the surface of earlier deposits, built up with a droplet-like morphology. This accumulation pattern resulted in a concave upper surface upstream, ending in a convex morphology, with steep

fronts and sides. Upstream from the terminal lobes, only the lateral *levées* recorded the path of the flows (Douillet *et al*., 2013). The surface exhibited lobes and *levées* covered with disk-shaped and vesicular large clasts. The deposits were massive and unsorted, containing clasts >1 m in diameter down to fine ash material. Lithics were prominent in the basal layer (~60 vol.%), but larger clasts never reached more than 40 vol.% in other layers, except if non-juvenile (*i.e.*, accessory and accidental) lapilli size material is incorporated to the current by erosion and bulking processes (Bernard *et al.*, 2014).

On the 2006 PDCs depositional fan, the deposits were laterally widespread (<600 m), with low snouts and no *levées*. Their outer surfaces were covered with juvenile clasts that mainly ranged from 15 to 25 cm in diameter (20-42%), accidental clasts (1-10%, but normally <2%), and a matrix (50-80%) of coarse-ash and lapilli (Fig. 3E, F). The most characteristic fragments were cauliflower bombs, broken and abraded during their emplacement, which form a major part of the coarse fraction of the PDC deposits. Within these channels, subsequent flow lobes were found as remnant pulses. Flow lobes were covered with <3 m cauliflower-shaped and planar or disk-shaped ("pancakes") bombs (Fig. 4D), some slightly vesiculated and rarely abraded, within a 45% coarse-ash matrix (Hall *et al*., 2013).

On top of the sequence, a dark gray PDC deposit had a prominent channel-and-levee morphology, and a notable abundance of large dark gray to black bombs, which were characteristically flattened or crushed as a disk-shaped cauliflower bomb (length and width are about five times the thickness) with a breadcrust texture (Fig. 3E, F). The lobes were clast-rich (30-80%) on their outer surfaces, but internal portions had a significant coarse-to-fine ash, a yellowish-brown matrix (40-70%) core and included accidental lithic material (5-10%). The inner part of the flattened bombs was rich in spherical or elongate bubbles, whereas the rim was denser, sometimes glassy, showing deep cracks. These oblate and fragile flattened bombs were sometimes intensely folded, but were found unbroken, sometimes more than 6 km away from the vent, above the lobe and levee surfaces. Full crushed cauliflower bombs were flatter than the broken pieces, but lithics appeared with the most spherical shapes (Douillet *et al*., 2013).

The different layers, in places separated by thin strata of ash interpreted as fallout deposits, are the result of different flows separated by pauses.

A total volume of the 2006 PDC deposits was estimated to $38.7\times10^6$ m$^3$. Of this total volume, nearly $30.5\times10^6$ m$^3$ is attributed to the juvenile contribution during the August 16-17 eruption (Hall *et al.*, 2013). The February 2014 PDCs were more variable in terms of their texture and facies, from *levées* composed of large cauliflower bombs to fine-depleted surfaces with large blocks, and also, a fine-rich surface with smaller lapilli clasts (Romero *et al*., 2017).

The PDCs in the last eruptive phase were formed by degassed lava spill-outs from the crater. The two largest PDCs occurred after midnight, probably generated by fountain collapse (Hall *et al*., 2013), like in the 1995 to 1999 eruptions at Montserrat (Druitt *et al*., 2002). However, the Vulcanian fountain collapse at Montserrat generated pumice ash flows, no BAFs or other coarse PDCs.

### *2.1.7. Fuego volcano, Guatemala*

Fuego (3,763 m a.s.l.) is one of the most active stratovolcanoes in Central America. The October 1974 eruptive cycle, of our particular interest, began on October 10 and involved four main episodes of PDC generation. The resulting deposits were massive, ungraded, unwelded, poorly sorted, and with variable amounts of dense juvenile blocks and bombs. The latter showed smooth to cauliflower surfaces and were embodied in a matrix of ash and matrix (Fig. 5). The flows were generally less than 2 m thick, but successions of PDCs produced deposits as much as 15 m thick with *levées* and overbanking areas. The PDCs traveled about 7 km from the vent at an average speed of 16.6 ms$^{-1}$ (Davies *et al*., 1978; Escobar, 2013). The total accumulative thickness for the 1970's PDC sequence may reach up to 80 m thick in channel filling facies, and up to 25 m in superimposed overbanking facies (Escobar, 2013).

The 1999-2013 PDC deposits were in fabric, components, and grain size distribution almost indistinguishable from the 1970's events. The 1999-2013 deposits consist of blocks and bombs, often 2-3 m in diameter, within a light to dark gray matrix of ash and lapilli, predominantly monolithologic, poorly sorted, non-stratified, and non-indurated. In some cases, the top of the deposits had a slight pink color. The bombs had a typical cauliflower surface, and sometimes displayed elongated and convoluted shapes. Although massive in general, some structures can be present as coarse tail grading, horizontal trains, or concentration of large clasts.

Flow units typically had a thickness of 2-5 m, but channel filling facies reached up to 10 m. Highly oxidized clasts corresponded to accidental lithics incorporated during transport. Elutriation pipes were uncommon in the channel filling facies but were frequent in overbanking facies. The main PDCs (*i.e.*, June 29 2003; July 17 2005; September 13 2012) were probably related to summit collapses of hot pyroclastic deposits (*i.e.*, spatter, scoria and bombs) near the active crater, contemporaneous with boiling-over eruptions. The total volume reached about $1.4\times10^8$ m$^3$ (Escobar, 2013).

The last, more recent, and well-studied biggest eruption at Fuego on June 3 2018, which lasted about 17 hours and produced an eruptive column that reached up to 16 km. The finest ashes traveled westwards for more than 40 km. The eruptive columns collapsed mainly towards the southeast flank of the volcano, where the PDCs (total volume of $15.1\pm4.2\times10^6$ m$^3$) traveled downstream confined to some of the existing gullies, causing catastrophic impacts (156 people died, 268 still missing, 186 houses destroyed, and 12,000 people evacuated). The largest PDC traveled 13 km from the active crater (World Bank, 2018[1]; Pardini *et al*., 2019). The June 3 PDCs deposits are characterized by the presence of several overlapping lobate deposits (at least 13 units), composed by dark-grey cauliflower bombs, grey dense blocks, and oxidized/hydrothermally altered clasts, in a coarse to fine lapilli-ash matrix and clast-supported fronts (Charbonnier *et al*., 2023).

### *2.1.8. Tilocálar Sur volcano, Chile*

In the Central Andes, in the southern part of the Atacama salar, there are two small volcanoes formed mainly by thick aphyric and phyric lava flows. The southern one of these two volcanoes, Tilocálar Sur (730-460 ka), consists of basal black to reddish brown agglutinated and moderately vesicular scoria deposits (up to 6.4 m thick) of andesitic composition, together with basaltic andesite and pyroxene andesite lava flows (Gardeweg and Ramírez, 1982; González *et al*., 2009; Ureta *et al*., 2021). Part of the deposits on the flanks are very coarse-grained and clast-supported, in which the main components are large cauliflower basaltic andesite bombs (up to 1.2 m in diameter) with reverse grading, set in a poorly sorted lapilli-rich matrix, 1-2.5 m thick. The deposits are locally welded (agglomerates and agglutinates), whereas in other sectors they are either incipiently welded or unconsolidated with imbricated structures. Ureta *et al*. (2021) interpreted this deposit as a near-vent fallout due to the predominance of aerodynamic-like clasts, in point-to-point contact. However, here we interpreted it as a PDC deposit because it has a clear imbricate structure, indicative of lateral transport slope-down, reverse grading, and autoclastic components into the bombs filling spaces (Fig. 5C).

### *2.1.9. Láscar volcano, Chile*

The Láscar composite volcano (5,592 m a.s.l.), located in northern Chile, some 70 km southeast from San Pedro de Atacama, is considered the most active volcano in the Central Andes (Amigo, 2021). In its flanks there is a late Middle to early Upper Pleistocene PDC deposit up to 3.7 km from the volcano's summit. Its thickness ranges from 5 to 20 m, locally reaching up to 35 m where at least nine flow units are observed. The PDC deposit is very coarse-grained, clast-supported to marginally matrix-supported, in which the main components are large cauliflower andesite bombs (0.1-2 m in diameter) set in a poorly sorted ashy scoriaceous matrix (Figs. 1B, C; 2). Most bombs are brick red in color but also black and are poorly-to-moderately vesicular (clast density 1,110-2,000 kg m$^{-3}$ with a mean of 1,460 kg m$^{-3}$) with a honeycomb texture. They are strongly welded, whereas in other sectors they are either incipiently welded or unconsolidated. Other two andesite PDC deposits, extending about 6 km on the southwest flanks from the source, are coarser grained than the previous ones and reach also up to 30 m in thickness. These deposits consist of dense (1.16 to 1.60 g cm$^{-3}$ with a mean density of 1.37 g cm$^{-3}$) clast-supported to marginally matrix-supported cauliflower rounded bombs (0.1-2 m) with a poorly sorted ashy matrix. In proximal outcrops there are abundant megaclasts (up to 10 m in diameter) of welded clastogenic lava and agglutinates (Gardeweg *et al*., 1998, 2011).

### *2.1.10. Aso volcano, Japan*

Aso volcano, in southwestern Japan, represents one of the largest calderas in the world. Post-caldera cones grew near the caldera center being the Nakadake volcano the only active cone (Miyabuchi, 2009).

[1] World Bank. 2018. Concatenated Volcanic Hazards Fuego crisis, June 3rd 2018. World Bank. http://documents.worldbank.org/curated/en/360901560919670273/Concatenated-Volcanic-Hazards-Fuego-Volcano-Crisis

The Izumikawa PDC deposit (~19 ka) forms a fan apron of about 1.9 km$^2$ which extends up to 5 km northeast from the summit of Nakadake. The total thickness ranges from 3.1 to 7 m, and has a bulk volume estimated at $9.4\times10^6$ m$^3$. The Izumikawa PDC deposit is divided into a black lower unit and a reddish-gray upper unit. The black lower unit is massive and chaotic, crudely reverse graded, and poorly sorted, with abundance of spherical to elongated cauliflower bombs (88-96% of the larger clast), and subangular to subrounded, poorly vesiculated to nonvesiculated, faceted juvenile lithic blocks (4-12%), set in a non-cohesive, black coarse-ash matrix (Fig. 5D). At one locality there is a 1 cm thick, well-sorted scoria lapilli overlain by a 2 cm thick, well-sorted coarse ash layer, both with identical petrography when compared to those of the bombs. The reddish-gray upper unit is massive and chaotic, crudely reverse graded, and matrix supported with subangular juvenile clasts (57-59%), bombs (24-29%) and accessory lithics (14-17%). The matrix particles are composed of juvenile crystals and rare non-juvenile fragments. The glass component in both units is characterized by typical subangular to subrounded blocky textures, poorly vesiculated in general, dominated by planar or conchoidal fracture surfaces with evidence of transport abrasion; some of them show fluidal textures as well (Miyabuchi *et al*., 2006).

#### *2.1.11. Fuego volcano, Guatemala*

Prehistoric PDC deposits (<4 ka) are very similar to historical PDC deposits at Fuego. That is, massive, poorly sorted deposits, consisting of an ash to lapilli-sized matrix with variable dense blocks and cauliflower bombs (Escobar, 2013).

#### *2.1.12. Tungurahua volcano, Ecuador*

On the western flank of Tungurahua, a series of prehistoric andesitic PDC deposits were identified and studied, some of them rich in scoria and cauliflower bombs, with ages ranging from >1,250 yr BP to 270 yr BP. The youngest PDC deposits are rich in cauliflower bombs as well, have runout distances of 5-7 km, and their deposits comprise ravine-ponded breccias associated to finer-grained overbanked diluted PDC layers (Fig. 5E). The deposits are poorly sorted, composed of angular to subangular non-juvenile blocks (10-60 cm in length) with variable dark andesitic cauliflower bombs with chilled margins, all inside a matrix similar in components to the largest clasts. Some subrounded lapilli pumices are also present (Le Pennec *et al*., 2008).

## 3. Discussion

Throughout this review, we found several key similarities between the different PDC deposits rich in cauliflower bombs (BoAF deposits). We summarize our main findings in table 1 and Fig. 6, and provide in this chapter an in-depth discussion about the main common aspects that can be used as a guide to future studies.

### 3.1. Deposit description, clast componentry, and erosion features

The BoAF deposits are massive (non-sorted and non-stratified), composed of non-indurated pyroclastic material, mainly cauliflower bombs and blocks, embedded in a matrix of lapilli and ash. The deposits can be clast-supported and matrix-supported, with lateral variations between the two, typically showing bimodal grain size distributions. The coarse juvenile clasts range from dense spatter to moderately vesicular scoria bombs to dense blocks. Their shapes are angular (juvenile blocks or broken bombs), ellipsoidal, spindle, discoidal, flat, and fusiform to highly irregular, although many clasts have one or more of these shapes. They can also have a faceted surface caused by brittle breakage, while some have thin chilled rinds surrounding a more vesicular interior, due to contact with air, water, or ice. In general, the BoAF deposits are composed by juvenile blocks (3-45 vol.%), bombs (20-60 vol.%), and non-juvenile blocks (1-10 vol.%), within a lapilli and ash depleted matrix (15-80 vol.%). The percentage of large (>6.4 cm in diameter) components also helps discriminating between BoAF and BAF deposits, where the BAF are poor in bombs and non-juvenile blocks (Fig. 6). Juvenile blocks are much less vesiculated than in BoAF deposits, and exhibit chiesel marks in their surfaces, produced by scratching with other blocks during transport (*i.e*., slickensides). The cauliflower-textured bombs can also be imbricated (Figs. 3F and 4D).

Although massive in general appearance, some poorly developed structures can be recognized in BoAF deposits. These include coarse tail grading (often reverse) and horizontal lenses of larger clasts

**TABLE 1. COMPARISON BETWEEN THE HISTORICAL BOAF DEPOSITS OBSERVED FOR SOME OF THE ERUPTIONS MENTIONED IN THE TEXT.**

| Volcano | Asama | Cotopaxi | Mayon | Spurr | Arenal | Tungurahua | Fuego |
|---|---|---|---|---|---|---|---|
| **Year** | 1783 | 1877 | 1968 | 1992 | 1975, 1993, 1998, 2000, 2001 | 2006, 2014 | 1974, 1999-2013, 2018 |
| **Clast type and textures** | Polytextural: cauliflower bombs and composite bombs | Polytextural: cauliflower bombs and blocks | Polytextural: cauliflower bombs and blocks | Polytextural: cauliflower bombs and blocks | Polytextural: cauliflower bombs and blocks | Polytextural: cauliflower bombs and blocks | Polytextural: cauliflower bombs and blocks |
| **Emplacement temperature of dilute PDC (°C)** | - | - | 100-400 | ~300 | 90-150 | ~100-300 | - |
| **Internal and/ or external structures** | Different flow and cooling units | Lobes | - | Lobes | Two gradational layers, no internal structure; lobes | Lobes | Different flow units |
| **Volume ($m^3$)** | $250\times10^6$ | $0.7\times10^6$ | $15\times10^6$ | $0.4\times10^6$ | $0.5\text{-}3\times10^6$ | $1.2\text{-}30\times10^6$ | $1.8\text{-}25.5\times10^6$ |
| **Number of flow units** | 6 (upper unit) | - | - | Several | 1-27 | ≥9-31 | Several |
| **Velocity ($m\ s^{-1}$)** | - | - | 9-63 | 6.1 | 11-33 | 3.5-36 | ≥10-40 |
| **Run-out length (km)** | 9 | 9.2 | ~4.4-5.0 | 3.2 | 2.0-3.6 | 10 | 3.2-13 |
| **Equivalent coefficient of friction (H/L)** | 0.15 | 0.24 | 0.4-0.45 | 0.46 | 0.28-0.46 | 0.29-0.36 | 0.31-0.41 |
| **References** | Yasui and Koyaguchi (2004) | Andrade *et al.* (2005) Pistolesi *et al.* (2011, 2013) | Moore and Melson (1969) | Miller *et al.* (1995) | Alvarado and Soto (2002) Cole *et al.* (2005) | Kelfoun *et al.* (2009) Hall *et al.* (2013, 2015) Romero *et al.* (2017) | Davies *et al.* (1978) Escobar (2013) World Bank (2018) |

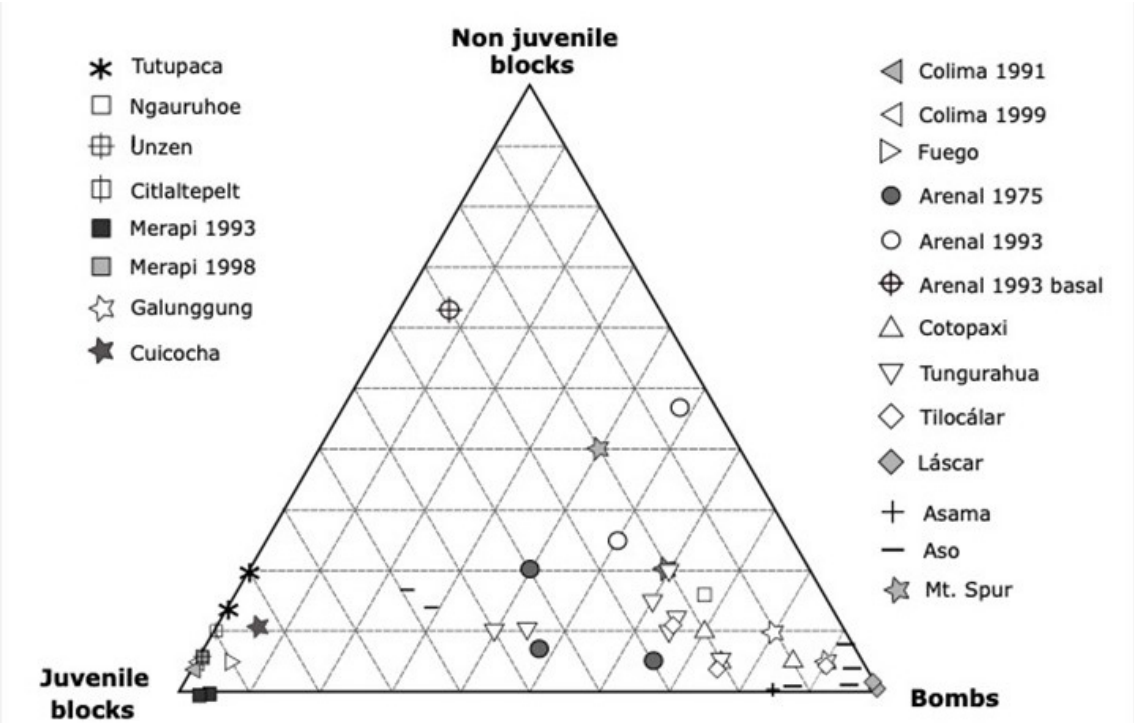


FIG. 6. Plot of major large components (juvenile and non-juvenile blocks and bombs) in a triangular diagram from different small-volume PDC deposits, in our case, typical examples of BAF and BoAF deposits from the literature and from our own descriptions (based on Davies *et al.*, 1978; Nairn and Self, 1978; Boudon *et al*., 1993; Miller *et al*., 1995; Gardeweg *et al*., 1998; Carrasco-Núnez, 1999; Fujii and Nakada, 1999; Saucedo *et al*., 2004; Yasui and Kiyaguchi, 2004; Schwarzkoft *et al*., 2005; Miyabuchi *et al*., 2006; Kelfoun *et al*., 2009; Sarocchi *et al*., 2011; Douillet *et al*., 2013; Hall *et al*., 2013; this work). The isolated sample from Arenal 1993 corresponds to the basal layer of the deposit, which is the first collapse of the crater wall, so it is rich in non-juvenile blocks. Surprisingly, there are few measurements or estimations of the percentage of bombs, juvenile and non-juvenile blocks in the literature for BAF and BoAF deposits.

(blocks or bombs), separating more homogenous and massive portions of the deposit, interpreted here as individual flow units. Density stratification during transport is usually considered because a dense granular flow may develop at the bottom, as well as an accompanying ash cloud, which has been fed by the escaping gas and finer elutriated particles (*e.g.*, Dufek *et al*., 2015; Brown and Andrews, 2015).

The surface features of the individual flow units include the presence of lobes at the terminus of individual pulses, lateral ridges, and *levées* (Fig. 3D, E and F). The 0.5-2 m tall *levées* at the top of the deposits are oriented parallel to the flow direction and are bomb rich. They form when the concentrated flow descends down the slopes and frictional forces are higher at the margins, particularly in flat-lying areas.

During high-velocity flows in historical cases, the bombs remained internally hot and fluidal, being ductile and gas-rich, and when the current come to rest, they deformed by collapse. Their ductile behavior is illustrated by the fact that some juvenile pieces that encountered obstacles along their path (*e.g.*, previous deposited blocks or standing trees), they engulfed or draped them. Thereafter, the vesiculation inside the bombs continued, but was restricted in the still-plastic, ductile crusts. Therefore, the bombs have chilled glassy crusts, although their surfaces are not smooth, having an intricate surface texture with many cracks. Many cauliflower bombs have vesicle-rich zones concentrated in open fractures. The surfaces of these open fractures are so fragile which suggests that vesiculation and expansion of the interior of the bombs must have continued

during the latest stages of transport, or after the flow settled down.

Here we propose that the faceted non-juvenile blocks were incorporated to the current from the crater wall margins or during transport (and erosion) of the current. The cauliflower to breadcrusted bomb morphology depends not only on the temperature, viscosity, and initial water concentration, but also on the cooling rate, which decreases due to air entrainment as the current evolves (Benage *et al*., 2014). An abundant fraction of clasts on *levées* and lobe surfaces, compared to inner parts of the deposit, is commonly observed (Alvarado and Soto, 2002; Hall *et al*., 2013), being interpreted as due to rafting of coarse clasts to the front and margins of the granular flow (Calder *et al*., 2000).

Deposit thicknesses range from 1 m for individual flow units, to more than 80 m for sequences of flow units aggregated over an entire eruptive episode, while deposit areas range between $10^5$ and $10^6$ $m^2$. Deposit volumes vary between $<10^5$ $m^3$ and $4\times10^7$ $m^3$ (Table 1). The ash elutriated from the current commonly falls on the flanks of the volcano, sometimes as accretionary lapilli as was the case of Mayon 1968 and Arenal 1993 BoAF-forming eruptions.

### 3.2. Petrography

In most of the studied cases, the bombs and juvenile blocks are porphyric basalts to andesites ($SiO_2$ content between 47.0-63.7 wt%; mostly <58.5 wt%), rich in phenocrysts (16-60%), particularly of plagioclase (12-51%) and clinopyroxene (2-3.10%), with variable orthopyroxene (0-4%), olivine (0-12.6%), and Fe-Ti oxides (0.5-3.9%). The mineralogy of the interstitial groundmass is identical to that of phenocrysts except that orthopyroxene and olivine are rare or absent (Rose *et al*., 1978; Gardeweg and Ramírez, 1982; Miller *et al*., 1995; Gardeweg *et al*., 1998, 2011; Alvarado and Soto, 2002; Yasui and Koyaguchi, 2004; Cole *et al*., 2005; Miyabuchi *et al*., 2006; Samaniego *et al*., 2011; Escobar, 2013; Romero *et al*., 2017; Ureta *et al.*, 2021). No dacite/rhyolite or andesite bearing amphibole, which are frequently reported for BAF deposits, have been so far reported in the studied cases of BoAF deposits. Thus, although a physical classification usually in most of the cases is not directly linked to composition, BoAFs apparently contrast BAFs, suggesting a rheological control related to the magma viscosity (Table 2).

### 3.3. Temperature, velocity, and mobility distances

The matrix of the BoAF deposits described here contained abundant shattered wood that varied from uncharred (*e.g.*, Arenal, Mt. Spurr) to uncharred/completely charred (*e.g.*, Fuego, Tungurahua). Several trees in direct contact with bombs were charred. The base of the deposit usually contains sediments with a reddish color, interpreted here as paleosols. Crude segregation pipes, reddish in color, indicate high temperatures as well (*e.g.*, Alvarado and Soto, 2002; Escobar, 2013; Hall *et al*., 2013). Bulk temperatures have been estimated at about 400 °C for some flows (Table 1), although single bombs (not include in Table 1) yield temperatures up to 1,000 °C Alvarado and Soto, 2002). The flows were very heterogeneous in temperature, with bombs remaining hot (>540 ºC) and lithics and ash deposited at much cooler temperatures (<100-300 °C), suggesting that these flows are efficient at entraining ambient air (Alvarado and Soto, 2002; Hall *et al.*, 2013; Dufek *et al*., 2015). Photographs, films, and eyewitness accounts analyzed here indicate that many BoAF clasts at Cotopaxi, Mayon, Arenal, Mt. Spurr, Tungurahua and Fuego volcanoes were incandescent, suggesting temperatures of about ≥700-1,000 °C (cf. Macdonald, 1972).

The PDCs were highly erosive in the upper valleys, particularly on steep higher flanks, as indicated by the presence of grooves and striations. In areas of high slope (>20º), the flows commonly groove, scratch, and polish the surfaces over, but in areas of lower slope (<15º) the flows tend to be depositional rather than erosional (Nairn and Self, 1978; Alvarado and Soto, 2002). In fact, in lower slope areas, the preexisting soil and/or dilute PDC deposited immediately before the arrival of the dense granular part of the flow are sometimes preserved. The lateral and frontal temperature of the dilute PDC was estimated to have been between 90 and 400 °C. Depending on the topographic relief of the terrain over which they flow and deposit, smaller volume flows ($<10^6$ $m^3$) are typically confined to narrow (30-300 m wide) and sometimes deep (up to 100 m) valleys, while larger volume flows ($>10^6$ $m^3$) are able to overbank smaller channels and destroy the adjacent interfluvial terrain. Some of these flows lie at the low-energy end of mass flows (c.f., Sheridan, 1979).

The BoAF velocities estimated (Table 1) varied from 9 to 63 $ms^{-1}$, mostly 20-40 $ms^{-1}$, typically for

**TABLE 2. PETROGRAPHIC COMPARISON OF THE JUVENILE CLASTS FOR BoAF DEPOSITS.**

| Volcano/ Eruption age(s) | Petrography: Phenocryst (%) and groundmass | $SiO_2$ wt% | Density (g $cm^{-3}$): Bomb (bo) Juvenile block (bk) Non-juvenile block (njbk) | Rock type | Morphology of matrix particles |
|---|---|---|---|---|---|
| Aso 19 ka | 35-40%: Plag+ol+cpx±opx intersertal | 49.6-51.4 | 1.6-2.5 (bo) 1.8-2.8 (jbk) 1.5-2.2 (njbk) | Porphyritic basalt | Most with typical blocky textures, poorly vesiculated, some with fluidal textures |
| Arenal 1993, 1998, 2000, 2001 | 30%: Plag+cpx+opx+Fe-Ti oxides; intersertal | 54.8-55.5 | 1.7-2.2 (bo) 1.8-2.3 (jbk) | Porphyritic basaltic andesite | Rounded vesicles (>20-35%) |
| Fuego 1974 | Plag+Px+Fe-Ti oxides; intersertal | 47.0-52.6 | - | Porphyritic basalt | Vesicles (20-47%) |
| Fuego 1999-2013 | Plag±px±ol | 48.0-54.0 | - | Porphyritic basalt to basaltic andesite | - |
| Asama 1783 | 18.5-30 %: Plag+cpx+opx+Fe-Ti oxides±ol; intersertal | 59.8-63.7 | - | Porphyritic andesite | - |
| Tungurahua 2006, 2014 | 16-29 %: Plag+cpx (± ol or opx); intersertal | 58.37-59.80 | - | Porphyritic andesite | Vesicles (31%) |
| Láscar Late Middle to early Upper Pleistocene | Plag+cpx±opx±ol; intersertal | 55.69-57.25 | 1.11-2.0 (bo) | Porphyritic basaltic andesite | - |
| Tilocálar Sur 760 ka | ≤2 %: Plag+cpx+ol+Fe-Ti oxides, rare hb; intersertal | 55.29-58.54 | - | Porphyritic basaltic andesite to andesite | Vesicles (30-80%) |

Source: Aso (Miyabuchi *et al*., 2006), Arenal (Alvarado and Soto, 2002; Cole *et al*., 2005), Fuego (Rose *et al*., 1978; Escobar, 2013), Láscar (Gardeweg *et al*., 1998), Tungurahua (Samaniego *et al*., 2011; Romero *et al*., 2017), Tilocálar Sur (Gardeweg and Ramírez, 1982; Ureta *et al*., 2018), and Asama (Yasui and Koyaguchi, 2004).

dense, low-volume currents (*e.g.*, Kelfoun *et al*., 2009) with limited run-out distances reaching up to 13 km, but mostly between 2 and 7 km from the active crater. The deposits halfway down vary from a very low fines content to highly matrix supported and are particularly coarse-grained (analogous to deposition from non-eruptive rock avalanches). The presence of surface *levées* and channels for unconfined small-volume PDC deposits, showing an almost massive internal structure, reverse grading, and a coarse ash matrix, all indicate that the mass flow was not highly fluidized, similar to dense granular flow regimes subjected to kinetic sieving and kinematic squeezing (Branney and Kokelaar, 2002; Félix and Thomas, 2004; Bursik *et al*., 2005; Lube *et al*., 2007).

Run-out distances vary from 2 to 7.5 km for small-volume PDC deposits, and the equivalent coefficient of friction or H/L (difference of elevation from the distal end of the deposit to the top of the crater versus the difference in altitude between the two; Shreve, 1968) varies between 0.13 and 0.46. A comparison of the mobility of the basal avalanches

related to BAFs and BoAFs was assessed using a plot H/L, including other type of deposits (Fig. 7). Francis *et al*. (1974) and Sparks (1976) were the first to note that small-volume PDCs, despite their high temperature, do not travel any further than air-supported cold rock avalanches (see also Carrasco-Núñez, 1999; Bursik *et al*., 2005; Schwarzkopf *et al*., 2005). In fact, regarding the mobility of the BAF and BoAF flows, vesicularity does not seems to play an important role. The gas phase is supposed to play only a subsidiary role in the transport dynamics of the dense part of PDCs, as the motion is dominated by dispersive and frictional stresses due to particle interaction, in a transport regime similar to concentrated granular flows (Alvarado and Soto, 2002; Felix and Thomas, 2004; Lube *et al*., 2007). For most of their transport, the bombs, and blocks travel by rolling and saltation with a strong interaction between particles, being an important mechanism in the hot, dense bed load region. Thus, even though vesiculation occurred during the transport of the current, the mobility of the flow was largely due to gravity, in part favored by air entrainment and the increase of the fluidity. Therefore, it is not necessary to postulate a high quantity of hot gases to explain the mobility of the BoAFs, although hot gases can have some contribution (Freundt *et al*., 2000; Alvarado and Soto, 2002; Hall *et al.*, 2013; Benage *et al*., 2014); in fact, in the case of Cotopaxi, Fuego and Asama, the relative unusually long runouts of some BoAFs (between >7.6 and 13 km; H/L=0.15-0.31) (Table 1) suggest that the mobility of the currents could have been enhanced by exsolution and expansion of magmatic gas from pyroclasts and entrainment of air, preferentially at the flow front. However, in general, BAFs and BoAFs are undistinguished in terms of H/L (Fig. 7).

### 3.4. Origin and mechanisms of emplacement of BoAFs

The internal and external structure of the cauliflower bombs, petrography, and surface textures,

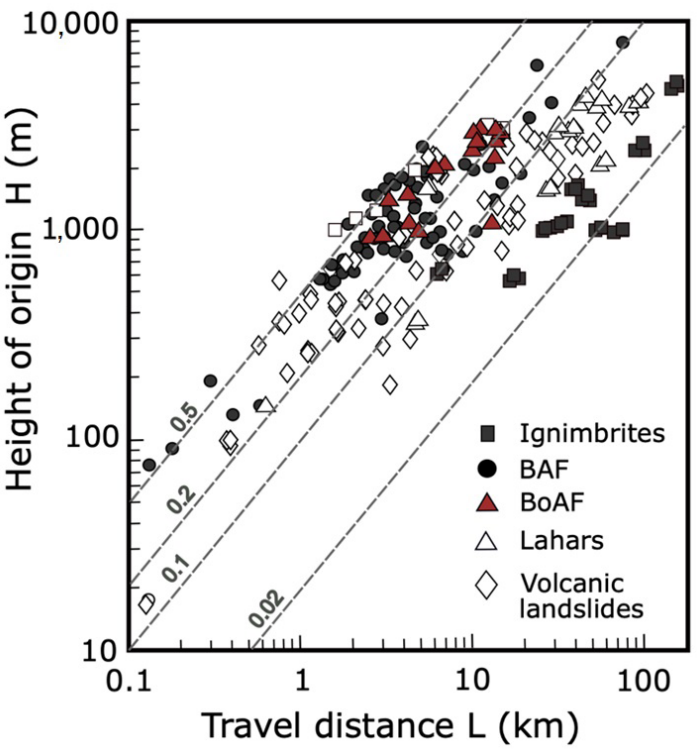


FIG. 7. Height drop (**H**) versus travelled horizontal distance (**L**) for BAFs and BoAFs. For comparison, recent analogous deposits and other gravity flows are also shown. Lines of equal H/L are depicted (based on Fisher and Schmincke, 1984; Yamamoto *et al*., 1993; Carrasco-Núñez, 1999; Freundt *et al*., 2000; Bursik *et al*., 2005; Romero *et al*., 2021; and this work).

as well as the internal fabric of the deposit and ash matrix are very similar for all the deposits described here, particularly for those at Fuego, Arenal, Cotopaxi, Tungurahua, Láscar, Mayon, Asama and Aso). For the PDC deposits studied here, no specific mechanisms are able to explain the abundance cauliflower bombs and their morphology, and their relationship with the observed eruption characteristics in volcanoes erupting relatively low silica products. Thus, could similar eruptive processes be assumed for the generation of BoAFs? or could different processes form similar deposits? Therefore, here we emphasize the three major mechanisms that may produce BoAFs: a) Partial collapse of the crater and the outpouring of the lava pool; b) Lava fountain and pyroclastic accumulation collapse; and c) Boiling-over eruptions.

#### *3.4.1. Partial collapse of the crater and the outpouring of the lava pool (Fig. 8A):*

Previous studies interpreted several small-volume PDC deposits rich in cauliflower bombs as BAF deposits. It was not until the work of Alvarado and Soto (2002) at the 1993 Arenal eruption, followed by Cole *et al*. (2005), then an alternative explanation was suggested. The most significant observation of the Arenal 1993 event was the partial collapse of the summit cone and the outpouring of a lava pool, without Strombolian explosions. A horseshoe-like opening (about 80 m depth) was present in the crater wall immediately after the event, within the area where intense fumarolic activity and repeated rockfalls had been observed two days before. A similar situation occurred during in 1975 (Alvarado and Soto, 2002). No horseshoe-like crater was formed in the 1998 event, but it was incipient in the 2000 and 2001 events, although the BoAF deposits are nearly indistinguishable from the 1993 BoAF deposit (Alvarado and Soto, 2002).

At Arenal (and could also be valid to other volcanoes), the explanation for the observed range in shapes and vesicularities in juvenile clasts, even within the same clast, is that they reflect varying degrees of cross-sectional heterogeneity due to heat and gas loss to the conduit wall, shear stress, crystallization and cooling of a near-solidus lava, open conduit dynamics, and veins prior to clast fragmentation. Thus, the fragments from the surface and margin of a lava conduit or lava pool, would presumably be cooler and denser than those from elsewhere. In fact, it is accepted that most of the juvenile clasts in the Arenal BoAF deposits came from the crust or cap of the top of the conduit or lava pool and sidewalls, representing molten fragments that burst from the interior of the lava conduit/pool and/or veins wrapped around some of the solidified fragments.

At Tungurahua, Hall *et al*. (2013, p. 89) describe typical solidified molten clots (*i.e.*, bombs) up to 50 cm in size rafted up onto flow *levées*, arguing that the so-called molten texture occurs on all sides of the clast, presumably due to air quenching, and not to a lava pool spill out. This was, however, not the case in Arenal, where the cauliflower bombs and quenching textures also occur, and the origin was the collapse and overflow of a lava pool. Nevertheless, later in the paper, Hall *et al*. (2013, p. 91) did mention that the molten clots could also have been formed by low-level lava fountaining or by spilling out of a lava pool in the waning stages of the eruption. Evidence of a small lava pool was interpreted by one of us (TT) from a fly-over of the crater at Tungurahua before the paroxysmal eruption in 2006.

At Láscar, some of the earlier PDC deposits (Gardeweg *et al*., 1998) resemble BoAF deposits. They contain little ash matrix, and the juvenile clasts show evidence that the magma had already been partially degassed. Additional evidence for an earlier stage of fragmentation and degassing, prior to PDCs formation, is evident in the clastogenic and brecciated textures, and in the high juvenile densities. Gardeweg *et al*. (1998) proposed that ascending andesite magma erupted into the crater and formed a deep lava pool filled with degassed lava, clastogenic lava breccias and coarse fallout agglutinates, suggesting that the lava pool became more viscous as it deepened, partly due to crystallization from the undercooled degassed lava. Thus, as the lava pool deepened, and became more viscous, new gas-rich magma was trapped at depth. Eventually gas pressure reached a critical threshold and an explosion disrupted the lava pool, ejecting much of the lava and forming a BoAF (Fig. 8A).

At Aso volcano, the Izumikawa ~19 ka PDC deposit is interpreted in this work as a BoAF-forming event related to lava pool or open conduit, although there is no clear additional field evidence for such assumption. However, at least for the upper flow unit, a crater-wall collapse was previously proposed (Miyabuchi *et al*., 2006). At Cotopaxi, according to additional historical records (*i.e.*, documents of

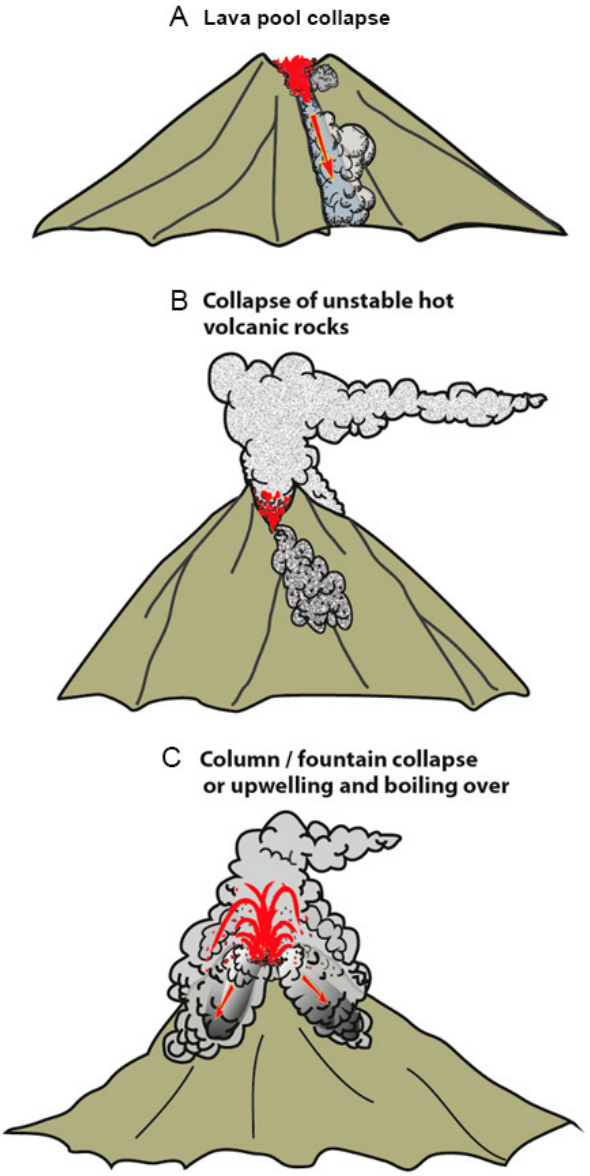


FIG. 8. Chart of representative different volcanic origins that could produce BoAF deposits according to the cited literature: **A**. crater collapse containing a lava pool, **B**. the gravitational collapse of hot unstable agglutinates, lava auto-breccias or hot tephra deposits and, **C**. the collapse of an eruption column or magma upwelling and boiling-over at the vent.

the priest Luigi Aloysius Sodiro in 1877 and Franz Theodor Wolf in 1878), it is possible to interpret the presence of lava (lava pool?) in the crater summit sometime before the climax of the 1877 eruption (Sodiro, 1877; Wolf, 1878). A similar situation was observed at Mayon in 1968 (Moore and Melson, 1969), where local reports described the appearance of a glow in the summit previous to the PDC-forming eruptions, which suggests the proximity of the lava and perhaps an ephemeral lava pool.

If the viscosity of the lava is too low, the drainage of the lava pool could generate a lava flow or lavafall, instead of a true PDC, as occurred during the 10 January 1977 eruption of Nyiragongo volcano (Democratic Republic of the Congo). Here, a low-viscosity lava flow with a volume of at least $20\times10^6$ m$^3$ drained from the lava lake

through fractures on the crater wall, flowing down the flanks of the volcano, destroying nearly 400 houses, and killing about 300 people (Tazieff, 1977, 1994).

#### *3.4.2. Lava fountain and pyroclastic accumulation collapse (Fig. 8B):*

Lava fountain in steep volcanoes and partial collapse of the scoria/agglutinate cone due its rapid growth is interpreted here to have played a significant role in the generation of the BoAF deposit and clastogenic lava flow at Asama in 1783 (Yasui and Koyaguchi, 2004). At Mt. Spurr, the distribution of PDC deposits indicates that they may have been generated by directed ballistic ejection and inclined column collapse (Miller *et al*., 1995). A similar origin is postulated for most of the 2006 PDCs at Tungurahua, related to intense fire fountaining collapse and/or to strong explosive bursts, some visually confirmed and/or recorded by a monitoring station. Other PDCs detected by instruments, but whose origin could not be related to discrete eruptive outbursts, were attributed to the sluffing off accumulated ejecta from the crater rim (Hall *et al*., 2013). In addition, lava fountains >600 m in height, and perhaps even 200-300 m in height, were also reported at Mayon in 1968 (Moore and Melson, 1969), and at Cotopaxi (Wolf, 1878), respectively. In both cases the still hot deposits rapidly collapsed by gravity, generating BoAFs.

The 2014 PDCs at Tungurahua were interpreted by Romero *et al*. (2017) as a result of upper flank loading with deposits from a vertically erupting column, and their subsequent destabilization, a mechanism quite similar to the 2006 PDCs described by Kelfoun *et al*. (2009). A similar interpretation was invoked for the Fuego 2018 eruption, where the generation of PDCs was due to the partial collapse of hot, recently accumulated pyroclastic material at and around the summit, involving a large volume of material and long (12-13 km) runout flows (Charbonnier *et al*., 2023). The February 11 2014 eruption at Etna is another example of a considerable volume (0.82 to $1.29\times10^6$ $m^3$) PDC (scoria flows) generated by of the collapse of unstable and hot pyroclastics from the lower flanks, which however have a no large juvenile componentry (Andronico *et al.*, 2018).

#### *3.4.3. Boiling-over (Fig. 8C):*

During the Cotopaxi 1877 eruption, T. Wolf described the eruption -very probably related to PDCs- as generated by "a dark foam-like cloud that boiled over the rim of the crater and descended all sides of the cone, much like a pot of cooking rice boiling over". This boiling-over PDC-forming model has been proposed for the BoAF events at Cotopaxi (Andrade *et al*., 2005; Pistolesi *et al.*, 2011, 2013) and Fuego (Escobar, 2013). Also, some of the PDCs observed in 2006 and 2010 at Tungurahua were interpreted as having been generated by boiling-over eruptions, one of which produced explosive fountaining but no significant convective plume. The boiling-over mechanism occurs when vesiculated magma fountains over the crater rim without forming a convective plume (Dufek *et al.*, 2015).

### 3.5. Some brief comments on volcanic hazards and monitoring

The results of our comparative study and compilation of several cases should help to better elucidate interpretations of other similar BoAF deposits elsewhere and can reasonably be used to help define the likely hazards associated with such events. BoAFs can be generated several days, weeks or even months after the beginning of explosive volcanic activity, showing little warning or previous signals, especially in those open-vent systems that transit rapidly from one eruptive style to the other, including paroxysmal explosive events. As the timing of a crater wall collapse or column collapse event cannot be reliably predicted, the best strategy for reducing risk to people and property is to minimize the settling within hazardous areas and to limit access to areas that could potentially be affected by BoAFs.

In general terms, both BoAFs and BAFs are similar in clast size distribution, velocity (impact force), temperature, and topographic channelization. They can also overbank topographic obstacles, meaning that they are able to affect more extensive areas, thus hazard assessment should be similar for both density currents.

A large area of the most hazardous zone for PDCs at Arenal and Cotopaxi is now inside their respective national parks, but outside these areas there is a large tourist development projects (*e.g.*, hotels, cabins, swimming pools, camping areas, touristic trails). Another is the well-known touristic area of "Baños de Agua Santa" near Tungurahua. Cotopaxi, although less visited by tourists, poses a high-risk related to lahars triggered by PDCs. In the same way, the Sensuikyo valley at Aso volcano, of the

most popular tourist destinations in Japan, is in the path of PDCs. The catastrophic PDC on June 3 2018 at Fuego volcano caused 424 deaths and missing people in a rural populated area. In summary, these mafic-to-intermediate Strombolian and frequent Vulcanian eruptions, which frequently are touristic attractions themselves, could also represent a risk for both local and external population.

In addition to traditional seismological, deformation and gas monitoring, the crystal textures of ash particles from Vulcanian and Strombolian eruptions can provide quantitative information about the dynamics of magma ascent and eruption that is otherwise difficult to obtain from other monitoring approaches (Toulkeridis *et al.*, 2015). Wright *et al.* (2012) reported that the crystallinity of erupted ash particles is controlled by the magma supply rate (MSR). Ash erupted during periods of high magma supply is substantially less crystalline than during periods of low magma supply, also suggesting that the observed transition from intermittent Vulcanian explosions at low MSR to more a continuous period of Strombolian eruptions and lava fountains at high MSR can be explained by the rise of bubbles through (Strombolian) or trapping of bubbles beneath (Vulcanian) vent-capping, variably viscous (and crystalline) magma. However, the PDC could occur without any premonitory or alert signal.

## 4. Conclusions

Here we described a number of PDCs rich in bombs, herein called BoAFs. BoAFs differ significantly from the more traditional BAFs. In the same way, the models of origin between the two also present some differences; for instance, the difference between the shapes of juvenile material is, in BoAF deposits, mostly due to their rheology and cooling histories.

Three mechanisms are proposed here as the most likely to generate BoAFs. The first one is due to a lava pool collapse. In this case, a poorly stratified lava reservoir is needed, which drains catastrophically when the containing rock walls fail (*i.e.*, crater wall collapse), resulting in the down-slope gravitational mass transport of the lava. The heterogeneous and stiffened lava will fragment and form a PDC if it is strained at a high enough rate during transport. The second mechanism begins with the ejection and near-vent accumulation of spatter and scoria, possibly during either fire fountaining or violent Strombolian activity. If the accumulation occurs on a steep enough slope, the deposit may become unstable, collapse and move rapidly downslope. The eruption may also generate a clastogenic lava flow by coalescence and agglutination of hot spatter from the fountain, which can experience brittle failure on steep slopes, collapsing and transforming into a PDC. The third mechanism involves a boiling-over process, in which a mixture of fragmented magma and gases at the vent fails does not become buoyant, collapsing on the flanks of the volcano.

The evidence shown here suggests that there is no mechanical difference between BAFs and BoAFs, being BoAFs a subset of the BAF. Thus, BoAFs would be at one end of the PDC-generating processes, characterized by a substantial contribution of juvenile material but with specific rheological states and fragmentation mechanisms. Geochemical and petrographic differences can be observed between BAFs and BoAFs however, being andesites to rhyolites abundant in for the former, and basalts to andesites abundant for the latter. Mafic compositions imply more common scoriaceous cauliflower textures.

## Acknowledgements

The Instituto Costarricense de Electricidad (ICE) provided all logistical support in Costa Rica during the early research at Arenal (particularly between 1993 and 2010). GEA thanks the staff of the Universidad San Francisco de Quito (Ecuador), for their assistance and hospitality during a field trip at Cotopaxi and Tunguragua volcanoes. Thanks to W. Balseca, G.J. Soto, W.G. Melson (r.i.p.), A. Gourgaud and R. Escobar, who contributed interesting discussions in field and additional information. J. Viramonte, F. Aguilera, and G. Ureta help in the visit at the Tilocálar Sur volcano (Chile) and their interesting discussions during the International Volcanological Field Course of the Central Andes in 2019 through ALVO (Latin America Association of Volcanology). P. Rowley, J.E. Romero and D. Bertin made very valuable comments on the draft. Last but not least, J.I. Quintana drew our volcanic schemes. The cooperation of the authors has been possible due to the Geo-Network of Latin American-German Alumni (GOAL) initiatives.

## References

Alvarado, G.E.; Soto, G.J. 2002. Pyroclastic flows generated by crater-wall collapse and outpouring of the lava pool of Arenal volcano, Costa Rica. Bulletin of Volcanology 63: 557-568. doi: https://doi.org/10.1007/s00445-001-0179-9

Amigo, Á. 2021. Volcano monitoring and hazard assessments in Chile. Volcanica 4 (S1): 1-9. doi: https://doi.org/10.30909/vol.04.S1.0120

Andrade, D.; Hall, M.; Mothes, P.; Troncoso, L.; Eissen, J.-P.; Samaniego, P.; Egred, J.; Ramon, P.; Rivero, D.; Yepes, H. 2005. Los peligros volcánicos asociados con el Cotopaxi. Instituto Geofísico. La Escuela Politécnica Nacional, Serie 3: 156 p., http://www.documentation.ird.fr/hor/fdi:010036189

Andronico, D.; Di Roberto, A.; De Beni, E.; Behncke, B.; Bertagnini, A.; Del Carlo, P.; Pompilio, M. 2018. Pyroclastic density currents at Etna volcano, Italy: The 11 February 2014 case study. Journal of Volcanology and Geothermal Research 357: 92-105. doi: https://doi.org/10.1016/j.jvolgeores.2018.04.012

Aramaki, S. 1956. The 1783 activity of Asama volcano. Part I. The Japanese Journal of Geology and Geography 27 (2-3): 189-229.

Aramaki, S. 1957. The 1783 activity of Asama volcano. Part II. The Japanese Journal of Geology and Geography 28 (1-3): 11-3.

Barberi, F.; Coltelli, M.; Frullani, A.; Rosi, M.; Almeida, E. 1995. Chronology and dispersal characteristics of recently (last 5000 years) erupted tephra of Cotopaxi (Ecuador): implications for long-term eruptive forecasting. Journal of Volcanology and Geothermal Research 69 (3-4): 217-239. doi: https://doi.org/10.1016/0377-0273(95)00017-8

Benage, M.; Dufek, J.; Degruyter, W.; Geist, D.; Harpp, K.; Rader, E. 2014. Tying textures of breadcrust bombs to their transport regime and cooling history. Journal of Volcanology and Geothermal Research, 274: 92-107. doi: https://doi.org/10.1016/j.jvolgeores.2014.02.005

Bernard, J.; Kelfoun, K.; Le Pennee, J.-L.; Vallejo, S. 2014. Pyroclastic flow erosion and bulking processes: comparing field-based vs. modeling results at Tungurahua volcano, Ecuador. Bulletin of Volcanology 76: 858. doi: https://doi.org/10.1007/s00445-014-0858-y

Boudon, G.; Camus, G.; Gourgaud, A.; Lajoie, J. 1993. The 1984 nuée-ardente deposits of Merapi volcano, Central Java, Indonesia: stratigraphy, textural characteristics, and transport mechanisms. Bulletin Volcanology 55: 327-342. doi: https://doi.org/10.1007/BF00301144

Branney, M.J.; Kokelaar, B.P. 2002. Pyroclastic density currents and the sedimentation of ignimbrites. Geological Society, Memoir 27: 144 p. London.

Brown, R.J.; Andrews, G.D.M. 2015. Deposits of Pyroclastic Density Currents. *In* The Encyclopedia of Volcanoes (Sigurdsson, H.; editor). Academic Press: 631-648. https://www.sciencedirect.com/science/article/pii/B9780123859389000365

Burgisser, A.; Bergantz, G.W. 2002. Reconciling pyroclastic flow and surge: the multiphase physics of pyroclastic density currents. Earth and Planetary Science Letters 202 (2): 405-418. doi: https://doi.org/10.1016/S0012-821X(02)00789-6

Bursik, M.; Patra, A.; Pitman, E.B.; Nichita, C.; Macías, J.L.; Saucedo, R.; Girina, O. 2005. Advances in studies of dense volcanic granular flows. Reports on Progress in Physics 68: 271-301. doi: https://doi.org/10.1088/0034-4885/68/2/R01

Calder, E.S.; Sparks, R.S.J.; Gardeweg, M.C. 2000. Erosion, transport and segregation of pumice and lithic clasts in pyroclastic flows inferred from ignimbrite at Lascar Volcano, Chile. Journal of Volcanology and Geothermal Research 104: 201-235. doi: https://doi.org/10.1016/S0377-0273(00)00207-9

Carrasco-Núnez, G. 1999. Holocene block-and-ash flows from summit dome activity of Citlaltépelt volcano, Eastern Mexico. Journal of Volcanology and Geothermal Research 88: 47-66. doi: https://doi.org/10.1016/S0377-0273(98)00110-3

Charbonnier, S.J.; Garin, F.; Rodríguez, L.A.; Ayala, K.; Cancel, S.; Escobar-Wolf, R.; Chigna, G.; Chun-Quinillo, C.; González, D.; Chigna, W.; Chun-Quinillo, K.; Mérida, R; Calder, E.S. 2023. Unravelling the dynamics and hazards of the June 3rd, 2018, pyroclastic density currents at Fuego volcano (Guatemala). Journal of Volcanology and Geothermal Research 436. doi: https://doi.org/10.1016/j.jolgeores.2023.107791

Cas, R.A.F.; Wright, J.V. 1987. Volcanic successions: Modern and ancient. Unwin Hyman Inc: 528 p. London.

Cole, P.D.; Fernandez, E.; Duarte, E.; Duncan, A.M. 2005. Explosive activity and generation mechanisms of pyroclastic flows at Arenal volcano, Costa Rica between 1987 and 2001. Bulletin of Volcanology 67: 695-716. doi: https://doi.org/10.1007/s00445-004-0402-6

Davies, D.K.; Quearry, M.W; Bonis, S.B. 1978. Glowing avalanches from the 1974 eruption of the volcano Fuego, Guatemala. Geological Society of American Bulletin 89: 369-384. doi: https://doi.org/10.1130/0016-7606(1978)89<369:GAFTEO>2.0.CO;2

Douillet, G.; Pacheco, D.; Kueppers, U.; Letort, J.; Tsang-Hing-Sun, E.; Nustillos, J.; Hall, M.L.; Ramon, P.; Dingwell, D.B. 2013. Dune bedforms produced by dilute pyroclastic density currents from the August 2006 eruption of Tungurahua volcano, Ecuador. Bulletin of Volcanology 75 (11). doi: https://doi.org/10.1007/s00445-013-0765-7

Druitt, T.H.; Young, S.R.; Baptie, B.; Bonadonna, C.; Calder, E.S.; Clarke, A.B.; Cole, P.D.; Harford, C.L.; Herd,

R.A.; Luckett, R.; Ryan, G.; Voight, B. 2002. Episodes of cyclic Vulcanian explosive activity with fountain collapse at Soufriere Hills Volcano, Montserrat. *In* The eruption of Soufriere Hills Volcano, Montserrat, from 1995 to 1999 (Druitt, T.H.; Kokelaar, B.P.; editors). Geological Society, Memoir 21: 281-306. London. doi: https://doi.org/10.1144/GSL.MEM.2002.021.01.13

Dufek, J.; Ongaro, T.E.; Roche, O. 2015. Pyroclastic Density Currents: Processes and Models. *In* The Encyclopedia of Volcanoes (Sigurdsson, H.; editor). Academic Press: 617-629. https://www.sciencedirect.com/science/article/pii/B9780123859389000353

Escobar, R.P. 2013. Volcanic processes and human exposure as elements to build a risk model for volcán Fuego, Guatemala. Ph.D. thesis (Unpublished), Michigan Technological University. https://digital commons.mtu.edu/etds/638

Félix, G.; Thomas, N. 2004. Relation between dry granular flow regimes and morphology of deposits: formation of levees in pyroclastic deposits. Earth and Planetary Science Letters 221: 197-213. doi: https://doi.org/10.1016/S0012-821X(04)00111-6

Fink, J.H.; Griffiths, R.W. 1998. Morphology, eruption rates, and rheology of lava domes: Insights from laboratory models. Journal of Geophysical Research: Solid Earth 103 (B1): 527-545. doi: https://doi.org/10.1029/97jb02838

Fisher, R.; Schmincke, H.-U. 1984. Pyroclastic Rocks. Springer: 472 p. Berlin.

Francis. P.W.; Roobol, M. J.; Walker, G.P.L.; Cobbold, P.R.; Cowaed, M. 1974. The San Pedro and San Pablo volcanoes of northern Chile and their hot avalanche deposits. Geologische Rundschau. 63: 357-388. doi: https://doi.org/10.1007/BF01820994

Freundt, A.; Wilson, C.N.J.; Carey, S.N. (2000). Ignimbrites and block-and-ash flow deposits. *In* Encyclopedia of Volcanoes (Sigurdsson, H.; editor). Academic Press: 581-599. New York.

Frimberger, T.; Andrade, S.D.; Weber, S.; Krautblatter, M. 2021. Modelling future lahars controlled by different volcanic eruption scenarios at Cotopaxi (Ecuador) calibrated with the massively destructive 1877 lahar. Earth Surface Processes and Landforms 46 (3): 680-700. doi: https://doi.org/10.1002/esp.5056

Fujii, T.; Nakada, S. 1999. The 15 September 1991 pyroclastic flows at Unzen Volcano (Japan): a flow model for associated ash-cloud surges. Journal of Volcanology and Geothermal Research 89: 159-172. doi: https://doi.org/10.1016/S0377-0273(98)00130-9

Gardeweg, M.C.; Ramírez, C.F. 1982. Geología de los volcanes del Callejón de Tilocálar, cordillera de los Andes-Antofagasta. *In* Congreso Geológico Chileno, No. 3: A111-A123. Antofagasta.

Gardeweg, M.C.; Sparks, R.S.J.; Matthews, S.J. 1998. Evolution of Lascar Volcano, Northern Chile. Journal of the Geological Society 155: 89-104. doi: https://doi.org/10.1144/gsjgs.155.1.0089

Gardeweg, M.C.; Amigo, Á.; Matthews, S.J.; Sparks, R.S.J., Clavero, J. 2011. Geología del volcán Láscar. Región de Antofagasta. Servicio Nacional de Geología y Minería, Carta Geológica de Chile, Serie Geología Básica 131: 40 p., 1 mapa escala 1:50.000. Santiago.

Giordano, G.; Cas, R.A.F. (2021). Classification of ignimbrites and their eruptions. Earth-Science Reviews 220. doi: https://doi.org/10.1016/j.earscirev.2021.103697

González, G.; Cembrano, J.; Aron, F.; Veloso, E.E.; Shyu, J.B.H. 2009. Coeval compressional deformation and volcanism in central Andes, case studies from northern Chile (23° S-24° S). Tectonics 28. doi: https://doi.org/10.1029/2009TC002538

Gourgaud, A.; Thouret, J.-C.; Bourdier, J.-L. 2000. Stratigraphy and textural characteristics of the 1982-83 tephra of Galunggung volcano (Indonesia): implications for volcanic hazards Journal of Volcanology and Geothermal Research 104: 169-186. doi: https://doi.org/10.1016/S0377-0273(00)00205-5

Green, J.; Short, N.M. 1971. Volcanic Landforms and surface features. Springer, Berlin.

Hall, M.L.; Steele, A.L.; Mothes, P.A.; Ruiz, M.C. 2013. Pyroclastic density currents (PDC) of the 16-17 August 2006 eruption of Tungurahua Volcano, Ecuador: geophysical registry and characteristics. Journal of Volcanology and Geothermal Research 265: 78-93. doi: https://doi.org/10.1016/j.jvolgeores.2013.08.011

Hall, M.L.; Steele, A.L.; Bernard, B.; Mothes, P.A.; Vallejo, S.X.; Douillet, G.A.; Ramón, P. A.; Aguaiza, S.X; Ruiz, M.C. 2015. Sequential plug formation, disintegration by Vulcanian explosions, and the generation of granular Pyroclastic Density Currents at Tungurahua volcano (2013-2014), Ecuador. Journal of Volcanology and Geothermal Research 306: 90-103. doi: https://doi.org/10.1016/j.jvolgeores.2015.09.009

Kelfoun, K.; Samaniego, P.; Palacios, P.; Barba, D. 2009. Testing the suitability of frictional behaviour for pyroclastic flow simulation by comparison with a well-constrained eruption at Tungurahua volcano (Ecuador). Bulleting of Volcanology 71(9): 1057-1075. doi: https://doi.org/10.1007/s00445-009-0286-6

Le Pennec, J.-L.; Jaya, D.; Samaniego, P.; Ramón, P.; Moreno, S.; Egred, J.; van der Plicht, J. 2008. The AD 1300-1700 eruptive periods at Tungurahua volcano, Ecuador, revealed by historical narratives, stratigraphy, and radio-carbon dating. Journal of

Volcanology and Geothermal Research 176: 70-81. doi: https://doi.org/10.1016/j.jvolgeores.2008.05.019

Lev, E.; Ruprecht, P.; Oppenheimer, C.; Peters, N.; Patrick M.; Hernández, P.A.; Spampinato, L.; Marlow, J. 2019. A global synthesis of lava lake dynamics. Journal of Volcanology and Geothermal Research 381: 16-31. doi: https://doi.org/10.1016/j.jvolgeores.2019.04.010

Lube, G.; Cronin, S.J.; Platz, T.; Freundt, A.; Procter, J.N.; Henderson, C.; Sheridan, M.F. 2007. Flow and deposition of pyroclastic granular flows: A type example from the 1975 Ngauruhoe eruption, New Zealand. Journal of Volcanology and Geothermal Research 161: 165-186. doi: https://doi.org/10.1016/j.jvolgeores.2006.12.003

Macdonald, G.A. 1972. Volcanoes. Prentice-Hall Inc: 510 p. New Jersey.

Mellors, R.M.; Sparks, R.S.J. 1991. Spatter-rich pyroclastic flows on Santorini, Greece. Bulletin of Volcanology 53: 327-342. doi: https://doi.org/10.1007/BF00280225

Miller, T.P.; Neal, C.A.; Waitt, R.B. 1995. Pyroclastic flows of the 1992 Crater Peak eruptions: distribution and origin. *In* The 1992 eruptions of Crater Peak Vent, Mount Spurr Volcano, Alaska (Keith, T.E.; editor).. United States Geological Survey Bulletin 2139: 81-87. Washington.

Miyabuchi, Y. 2009. A 90,000-year tephrostratigraphic framework of Aso Volcano, Japan. Sedimentary Geology 220: 169-189. doi: https://doi.org/10.1016/j.sedgeo.2009.04.018

Miyabuchi, Y.; Watanabe, K.; Egawa, Y. 2006. Bomb-rich basaltic pyroclastic flow deposit from Nakadake, Aso Volcano, southwestern Japan. Journal of Volcanology and Geothermal Research 155 (1-2): 90-103. doi: https://doi.org/10.1016/j.jvolgeores.2006.02.007

Moore, J.G.; Melson, W.G. 1969. Nuées Ardentes of the 1968 Eruption of Mayon Volcano, Philippines. Bulletin of Volcanology 33: 600-620. doi: https://doi.org/10.1007/BF02596528

Murcia, H.F.; Borreo, C.A.; Pardo, N.; Alvarado, G.E.; Arnosio, M.; Scolamacchia, T. 2013. Depósitos volcaniclásticos: Términos y conceptos para una clasificación en español. Revista Geológica de América Central 48: 15-39.

Nairn, I.A.; Self, S. 1978. Explosive eruptions and pyroclastic avalanches from Ngauruhoe in February 1975. Journal of Volcanology and Geothermal Research 3: 39-60. doi: https://doi.org/10.1016/0377-0273(78)90003-3

Pardini, F.; Queir, M.; Maismith, A.; Watson, I.M.; Clarisse, L.; Burton, M.R., 2019. Initial constraints on triggering mechanisms of the eruption of Fuego volcano (Guatemala) from 3 June 2018 using IASI satellite data. Journal Volcanology and Geothermal Research 376: 179-194. doi: https://doi.org/10.1016/j.jvolgeores.2019.03.014

Pistolesi, M.; Rosi, M.; Cioni, R.; Cashman, K.V.; Rossotti, A.; Aguilera, E. 2011. Physical volcanology of the post-twelfth-century activity at Cotopaxi Volcano, Ecuador: behavior of an andesitic central volcano. Geological Society of America Bulletin 123: 1193-1215. doi: https://doi.org/10.1130/B30301.1

Pistolesi, M.; Cioni, R.; Rosi, M.; Cashman, K.V.; Rossotti. A.; Aguilera, E. 2013. Evidence for lahar-triggering mechanisms in complex stratigraphic sequences: the post-twelfth century eruptive activity of Cotopaxi Volcano, Ecuador. Bulletin Volcanology 75: 698. doi: https://doi.org/10.1007/s00445-013-0698-1

Romero, J.E.; Douillet, G.A.; Vallejo, S.; Bustillos, J.; Troncoso, L.; Díaz, J.; Ramón, P. 2017. Dynamics and style transition of a moderate, Vulcanian-driven eruption at Tungurahua (Ecuador) in February 2014: pyroclastic deposits and hazards considerations. Solid Earth 8: 697-719. doi: https://doi.org/10.5194/se-8-697-2017

Romero, J.E.; Polacci, M.; Watt, S.; Kitamura, S.; Tormey, D.; Sielfeld, G.; Arzilli, F.; La Spina, G.; Franco, L.; Burton, M.; Polanco, E. 2021. Volcanic lateral collapse processes in mafic arc edifices: a review of their driving processes, types and consequences. Frontiers in Earth Science 9: doi: https://doi.org/10.3389/feart.2021.639825

Rose, W.I; Anderson, A.T.; Woodruff, L.G.; Bonis, S.B. 1978. The October 1974 basaltic tephra from Fuego volcano: description and history of the magma body. Journal of Volcanology and Geothermal Research 4: 3-53. doi: https://doi.org/10.1016/0377-0273(78)90027-6

Samaniego, P.; Le Pennec, J.L.; Robin, C.; Hidalgo, S. 2011. Petrological analysis of the pre-eruptive magmatic process prior to the 2006 explosive eruptions at Tungurahua. Journal of Volcanology and Geothermal Research 199: 69-84. doi: https://doi.org/10.1016/j.jvolgeores.2010.10.010

Sarocchi, D.; Sulpizio, R.; Macías, J.L.; Saucedo, R. 2011. The 17 July 1999 block-and-ash flow (BAF) at Colima Volcano: New insights on volcanic granular flows from textural analysis. Journal of Volcanology and Geothermal Research 204: 40-56. doi: https://doi.org/10.1016/j.jvolgeores.2011.04.013

Saucedo, R.; Macías, J.L.; Bursik, M. 2004. Pyroclastic flow deposits of the 1991 eruption of Volcán de Colima, México. Bulletin of Volcanology 66: 291-306. doi: https://doi.org/10.1007/s00445-003-0311-0

Schwarzkopf, L.M.; Schmincke, H.-U.; Cronin, S.J. 2005. A conceptual model for block-and-ash flow avalanche transport and deposition, based on deposit architecture of 1998 and 1994 Merapi flows. Journal of Volcanology and Geothermal Research 139: 117-134. doi: https://doi.org/10.1016/j.jvolgeores.2004.06.012

Sheridan, M.F. 1979. Emplacement of pyroclastic flows: A review. *In* Ash flow tuffs (Chapin, C.E.; Elston, W.E.; editors). Geological Society of America Special Paper 180: 125-136.

Shreve, R.L. 1968. The Blackhawk landslide. Geological Society of America Special Paper 108: 1-47. doi: https://doi.org/10.1130/SPE108-p1

Sodiro, L. 1877. Relación sobre la erupción del Cotopaxi acaecida el día 26 de Junio de 1877. Imprenta Nacional: 40 p. Quito.

Sparks, R.S.J. 1976. Grain size variations in ignimbrites and implications for the transport of pyroclastic flows. Sedimentology 23:147-188. doi: https://doi.org/10.1111/j.1365-3091.1976.tb00045.x

Sulpizio, R.; Dellino, P.; Doronzo, D.M.; Sarocchi, D. 2014. Pyroclastic density currents: state of the art and perspectives. Journal of Volcanology and Geothermal Research 283: 36-65. doi: https://doi.org/10.1016/j.jvolgeores.2014.06.014

Tazieff, H. 1977. An exceptional eruption: Mt. Nyiragongo, Jan. 10th, 1977. Bulletin of Volcanology 40: 189-200. doi: https://doi.org/10.1007/BF02596999

Tazieff, H. 1994. Permanent lava lakes: observed facts and induced mechanisms. Journal of Volcanology and Geothermal Research 63: 3-11. doi: https://doi.org/10.1016/0377-0273(94)90015-9

Toulkeridis, T.; Arroyo, C.R.; Cruz D'Howitt, M.; Debut, A.; Vaca, A.V.; Cumbal, L.; Aguilera, E. 2015. Evaluation of the initial stage of the reactivated Cotopaxi volcano-analysis of the first ejected fine-grained material. Natural Hazards and Earth System Sciences Discussions 3 (11): 6947-6976. doi: https://doi.org/10.5194/nhessd-3-6947-2015

Toulkeridis, T.; Zach, I. (2017). Wind directions of volcanic ash-charged clouds in Ecuador-implications for the public and flight safety. Geomatics, Natural Hazards and Risk 8 (2): 242-256. doi: https://doi.org/10.1080/19475705.2016.1199445

Ureta, G.; Németh, K.; Aguilera, F.; Kósik, S.; González, R.; Menzies, A.; González, C.; James, D. 2021. Evolution of a magmatic to a phreatomagmatic volcanic system: The birth of a monogenetic volcanic field, Tilocálar, volcanoes, northern Chile. Journal of Volcanology and Geothermal Research 414. doi: https://doi.org/10.1016/j.jvolgeores.2021.107243

Wolf, T. 1878. Memoria sobre el Cotopaxi y su última erupción acaecida el 26 de junio de 1877. Imprenta del Comercio: 64 p. Guayaquil.

Wright, J.V.; Smith, A.L.; Self, S. 1980. A working terminology of pyroclastic deposits Journal of Volcanology and Geothermal Research 8: 315-336. doi: https://doi.org/10.1016/0377-0273(80)90111-0

Wright, H.; Cashman, K.; Mothes, P.; Hall, M.; Ruiz, A.; Le Pennec, J.-L. 2012. Estimating rates of decompression from textures of erupted ash particles produced by 1999-2006 eruptions of Tungurahua volcano, Ecuador. Geology 40: 619-622. doi: https://doi.org/10.1130/G32948.1

Yamamoto, T.; Takarada, S.; Suto, S. 1993. Pyroclastic flows from the 1991 eruption of Unzen volcano, Japan. Bulletin of Volcanology 55: 166-175. doi: https://doi.org/10.1007/BF00301514

Yasui M; Koyaguchi, T. 2004. Sequence and eruptive style of the 1783 eruption of Asama Volcano, central Japan: a case study of an andesitic explosive eruption generating fountain-fed lava flow, pumice fall, scoria flow and forming a cone. Bulletin of Volcanology 66; 243-262. doi: https://doi.org/10.1007/s00445-003-0308-8

Manuscript received: February 02, 2023; revised/accepted: July 19, 2023; available online: July 28, 2023.